Bubble Columns

For other industrial reactors and their applications, see → Stirred-Tanc and Loop Reactors, → Tubular Reactors, → Fixed-Bed Reactors, → Fluidized-Bed Reactors, → Three-Phase Trickle-Bed Reactors, → Reaction Columns, → Thin-Film Reactors, → Metallurgical Furnaces, and → Biochemical Engineering.

PETER ZEHNER, BASF Aktiengesellschaft, Ludwigshafen, Federal Republic of Germany

MATTHIAS KRAUME, BASF Aktiengesellschaft, Ludwigshafen, Federal Republic of Germany

Symbols (see also → Principles of Chemical Reaction Engineering and → Model Reactors and Their Design Equations)

Variables

a	specific interfacial area, m^{-1}
A	interfacial area, m^2
d	diameter, m
d_h	diameter of holes, m
d_i	inner diameter of draft tube, m
d_n	nozzle diameter, m
D	diffusion or dispersion coefficient, m^2/s
$D_{G,L}$	diffusion coefficient of dissolved gas in liquid, m^2/s
e_M	energy dissipation rate per unit mass, W/kg
e_n	jet power per unit volume, W/m^3
e_V	energy dissipation rate per unit volume, W/m^3
f	fraction of cross-sectional area
f_i	fraction of cross-sectional area of draft tube
F	cross-sectional area, m^2
F_i	cross-sectional area of draft tube, m^2
F_R	cross-sectional area of reactor, m^2
h	height, m
h_R	height of gas – liquid mixture, m
h_t	height of reactor, m
J_D	dispersion flow
k_L	liquid-phase mass-transfer coefficient, m/s
P	power, W
r	radial distance from column axis, m
t	time, s
u	superficial velocity, m/s
v	velocity, m/s
v_{rG}	relative velocity of bubble swarm in liquid, m/s
v_{rS}	relative velocity of particle swarm in liquid, m/s
V	volume, m^3
$\dot{V}$	volumetric flow rate, m^3/s
z	axial coordinate, m

10.1002/14356007.b04_275

Greek symbols

α	heat-transfer coefficient, $W\,K^{-1}\,m^{-2}$
ε	volume fraction
ε_G	gas holdup
ζ	drag coefficient of circulation flow
η	dynamic viscosity, $kg\,m^{-1}\,s^{-1}$
ν	kinematic viscosity, m^2/s
ϱ	density, kg/m^3
$\Delta\varrho$	density difference between liquid and gas, kg/m^3
$\Delta\varrho_S$	density difference between liquid and solids, kg/m^3
σ	surface tension, N/m
φ	mass concentration, kg/m^3

Subscripts

a	annular space
b	bubble
bS	Sauter diameter
c, circ	circulation
D	downflow
G	gas phase
h	hole
i	inside draft tube
L	liquid
max	maximum value
min	minimum value
M	per unit mass
n	nozzle
p	particle
r	relative
R	upflow, reaction mixture
slip	slip
S	solids
t	reactor
V	per unit volume

1. Introduction

Bubble columns are devices in which gas, in the form of bubbles, comes in contact with liquid. The purpose may be simply to mix the liquid phase. Far more often, however, substances are transferred from one phase to the other, for example, when gaseous reactants are dissolved in a liquid or when liquid reaction products are stripped. Both processes can take place simultaneously. A chemical or biological reaction nearly always proceeds in the liquid phase. Depending on the application, special measures to intensify mass transfer between the two phases may be useful, or the residence-time distribution of one or both phases may be modified.

The liquid may also contain inert, catalytically active, or reactive particles in suspension. Oxidation, hydrogenation, chlorination, phosgenation, alkylation, and other processes have long been performed in bubble-column reactors in the chemical industry. In 1978, more than 10^7 t/a of chemical products were made in bubble columns [1]. Since then, marked growth has occurred. Industrial reactors for high-tonnage products have capacities of 100 – 300 m^3. Larger bubble columns, with capacities up to 3000 m^3, are employed as fermenters for protein production from methanol. The largest units (20 000 m^3) are those for wastewater treatment.

Scientific interest in bubble columns has increased considerably in the past 10 – 15 years. Up to the mid-1970s, only 10 to 20 publications appeared annually; by the mid- to late 1980s, the number had increased to 80 per year. This led to the development of many empirical correlations and theoretical models enabling the mathematical simulation of bubble- column reactors. Some academic research groups and commercial software developers have offered simulation programs.

The mixing of a liquid and a gas having only partial mutual solubility is one of the unit operations in chemical technology. As Figure 1 shows, this operation takes one of three principal forms. The simplest design is the *bubble column* (Fig. 1 A) in which gas is fed into the column at the bottom and rises in the liquid, escaping from it at the upper surface; the gas is consumed to a greater or lesser extent (depending on the intensity of mass transfer and chemical reaction). When the off-gas contains high concentrations of valuable reactants, part of it is recycled to the reactor. This recycle design, however, lowers the concentration profile in the bubble column and must be optimized from an economic standpoint. In a simple bubble column the liquid is led in either cocurrently or countercurrently to the upward gas stream and has a long residence time. The flow direction of the liquid phase has little effect on the gas-phase residence time, which is comparatively short. Thus, in the

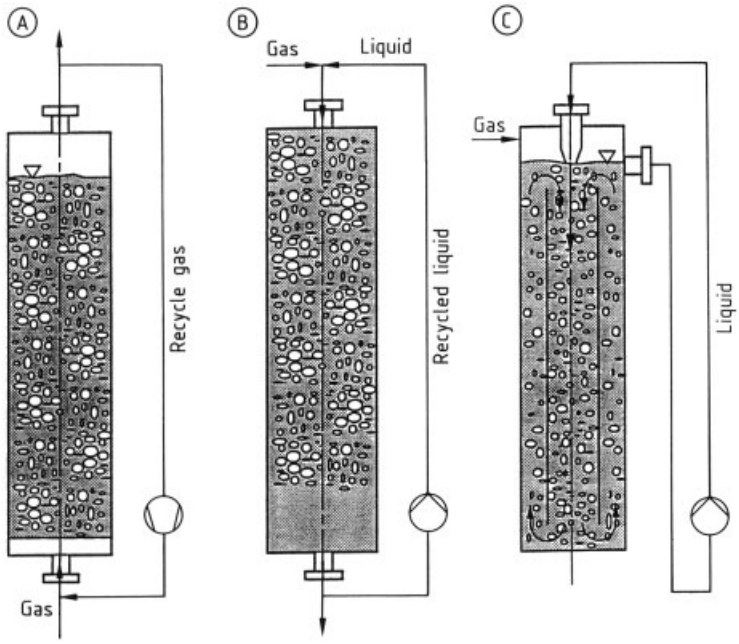

Figure 1. Principal methods of gas – liquid mixing
A) Bubble column; B) Downflow bubble column; C) Jet loop reactor

simple column, the flow of gas is always from bottom to top, and the stream can be made up of both fresh and recycle gas.

Longer gas-phase residence times can be achieved with the *downflow bubble column* shown in Figure 1 B. The liquid is pumped down through the column at a velocity of more than 20 cm/s, so that gas let in at the top is entrained in the flow and can even be held in a suspension-like state until it has reacted completely. Usually, however, unconsumed gas is removed with the liquid and separated. Special designs permit phase separation inside the apparatus. The downflow bubble column is used mainly when large liquid streams are to be contacted with small gas streams and a short liquid residence time is required. The necessary velocity cannot always be obtained with the liquid inlet to the reactor. Thus, like the gas in an ordinary bubble column, the liquid in the downflow bubble column can be recycled. Typical applications for downflow bubble columns are the ozonation of drinking water and the treatment of water in swimming pools. A special use of such devices in the evacuation and compression of gases has also been reported [2].

In both types of column energy must be supplied continuously to the two-phase system to keep the liquid and gas mixed. Only in this way can separation of the phases be counteracted or reversed. In the first case, the simple bubble column, this energy is supplied by the gas. In the downflow bubble column the energy is supplied by the downflowing liquid.

A different mechanism comes into play in the *jet loop reactor* (Fig. 1 C). Here no net flow of gas or liquid occurs along the column; instead, an internal circulating flow is produced. One way to achieve this is with a propeller, but other approaches exist. In the most commonly used type of loop reactor, the *jet loop reactor*, the flow is driven by a high-velocity liquid jet. As in the downflow bubble column, gas is let in at the top and dispersed by the jet energy. Bubbles can be distributed throughout the reactor volume only if the downward liquid flow velocity in the internal tube is greater than the slip velocity of the bubbles. Accordingly, a minimum power input is required.

These three basic methods of dispersing gas in liquid are generally not used in their pure forms. The variety of problems in chemical and biotechnical processes has led to many different contacting devices that combine these basic techniques.

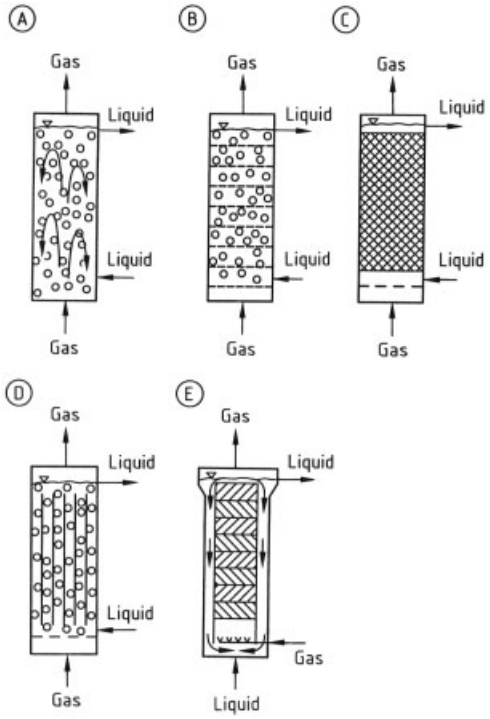

Figure 2. Types of bubble-column reactors
A) Simple bubble column; B) Cascade bubble column with sieve trays; C) Packed bubble column; D) Multishaft bubble column; E) Bubble column with static mixers

2. Bubble Columns and Modifications

2.1. Design and Applications

Bubble columns are very adaptable gas – liquid contacting devices; possible designs are shown in Figure 2. The simplest form of bubble column (Fig. 2 A) consists of a vertical tube with no internals. Gas is fed in at the bottom while liquid is led through the apparatus cocurrently or countercurrently. This simple form is seldom used in practice; instead, a number of modifications are employed. The back-mixing of gas and liquid phases in the simple bubble column and the nonuniform distribution of gas bubbles over the cross section can be reduced by the installation of trays (Fig. 2 B), packings (Fig. 2 C), or shafts (Fig. 2 D). All these devices can operate either cocurrently or countercurrently. To set up the most homogeneous possible bubble flow, static mixer elements can also be placed in the ascending flow section (Fig. 2 E).

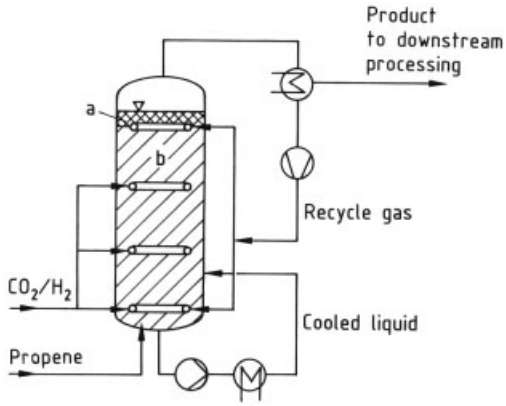

Figure 3. Hydroformylation of propene
a) Stripping zone; b) Reaction zone

Hydroformylation. The hydroformylation of propene is carried out in simple bubble columns. The reaction is homogeneously catalyzed by rhodium complexes. Usually the propene and the CO/H_2 gas mixture are let in at the bottom of the reactor. Incompletely reacted gas, saturated with the reaction product, exits the reactor. The hydroformylation product is separated from the gas stream by condensation and forwarded to downstream processing, while the gas is recycled to the reactor. Because the heat of reaction cannot be completely removed by evaporative cooling using the enthalpy of vaporization of the product, the bubble column is also equipped with an external cooling loop.

One great advantage of the process is that the product is recovered from the reaction mixture without additional separation operations which would damage the expensive catalyst system. The close coupling between the product and the recycle gas necessary to discharge it (i.e., a certain quantity of gas is required for product discharge for thermodynamic reasons), however, presents some problems. First, the gas flow rate causes a high gas holdup, which reduces the reaction volume and thus decreases the productiv-

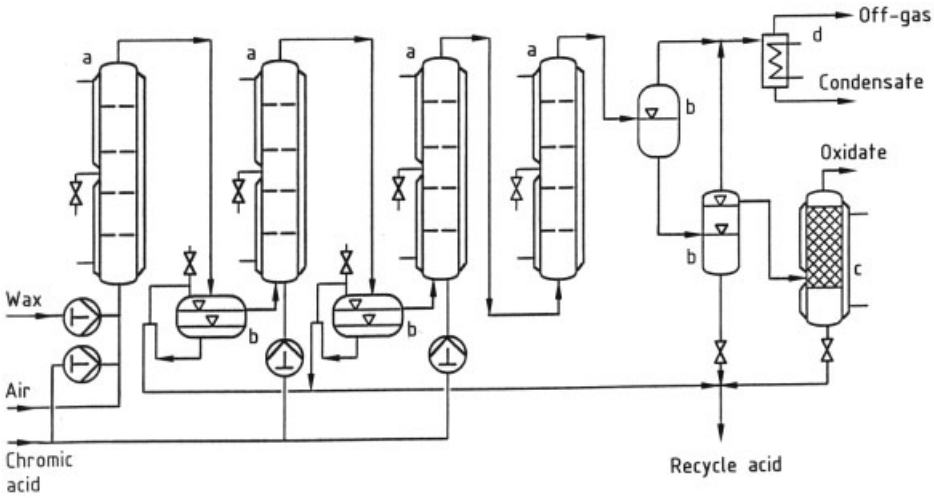

Figure 4. Oxidation of montan waxes in cascade bubble columns
a) Cascade bubble-column reactors; b) Separators; c) Final purification of wax oxidate; d) Off-gas treatment

ity of the reactor. Second, large bubbles occur, which limit the delivery of gaseous reactants to the liquid phase in the reactor. For these reasons, recycle gas is admitted to the bubble column at two levels (Fig. 3) [3]. About half of the recycle gas is fed via the bottom sparger to disperse reactants into the overlying reaction zone. The remaining recycle gas is let in via the top sparger, which lies slightly below the liquid surface, to facilitate separation of the reaction product. Finally, the CO/H_2 reactant stream is fed at various levels to supply CO that has been consumed by the reaction in the liquid phase.

Oxidation of Montan Waxes. Bubble columns are used in a cascade when a narrow residence-time distribution is required, for example, to prevent or limit undesired consecutive reactions. Reducing back-mixing (i.e., a narrow residence-time distribution) is also useful when reaction-engineering considerations dictate that the gas must be fed to various points in the reactor or when a liquid reactant must be degraded to the greatest extent possible.

Montan waxes from brown coal must be deresinified, oxidatively bleached, and esterified (optional) [4], [5]. Oxidation of the waxes consists of several consecutive reactions; the first three steps (oxidation of resins and dark- colored substances, saponification of montan waxes, oxidation of wax alcohols) are desirable, whereas the fourth (oxidative degradation of wax acids) is not. The residence-time distribution in the reactor must be controlled so that the desired reactions go as far as possible without the undesirable reaction occurring to any marked extent. Oxidation is performed in four cascaded bubble columns connected in series (Fig. 4). In the first bubble column, the crude wax for bleaching is metered in along with half of the required amount of chromic acid. Air is supplied to enhance mixing of the reactants. The spent chromic acid is separated from the wax downstream of both the first and the second bubble columns. Another 25 % of the total acid required is added to the second and third columns. The reaction preferably takes place at 100 – 125 °C and 1 – 5 bar, with a residence time of 1 – 3 h for the entire cascade. The enthalpy of reaction is removed by partial evaporation of the water contained in the chromic acid. After exiting the fourth bubble column, the oxidized product, spent acid, and off-gas are separated in two separators.

2.2. Gas Distribution

Usually, the gas is dispersed to create small bubbles and distribute them uniformly over the cross section of the equipment to maximize the intensity of mass transfer. The formation of fine bubbles is especially desirable in coalescence-hindered systems and in the homogeneous flow

regime (Section 2.3). In principle, however, significant mass transfer can be obtained at the gas distributor through a high local energy-dissipation density [6], [7].

In most cases, gas bubbles are generated by pores or holes or in the shear zone of a liquid jet. Figure 5 shows typical forms of *"static" gas spargers*, in which bubble formation occurs without any additional energy supplied from outside. The simplest of these devices, the *dip tube* (Fig. 5 A), only gives an acceptably uniform gas distribution over the cross section at some distance above the sparger. *Perforated plates* (Fig. 5 B) and *perforated ring spargers* (Fig. 5 C) are more effective. Both of these require a certain minimum gas flow rate to achieve uniform distribution and prevent the liquid from getting into the sparger [8–10]. Very fine bubbles can be generated by the use of porous plates (Fig. 5 D), but their pores are susceptible to fouling, and this type of sparger is seldom used in full-scale equipment.

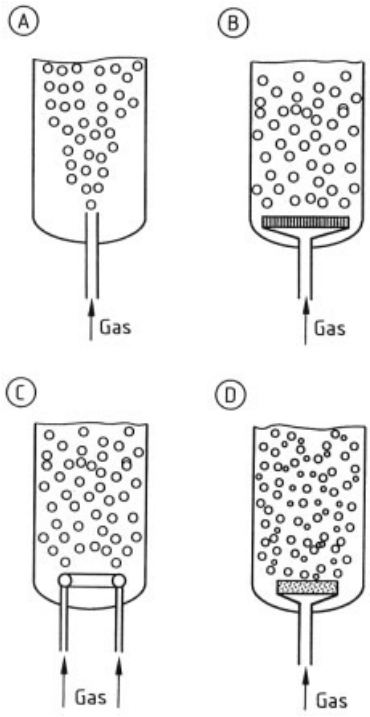

Figure 5. Static gas spargers
A) Dip tube; B) Perforated plate; C) Perforated ring sparger; D) Porous plate

Dynamic spargers offer an alternative to the static types. They use the power of a liquid jet to disperse gas in a zone of high energy-dissipation rate [11–13]. Figure 6 illustrates several frequently used dynamic gas spargers. The simple two-phase jet nozzle alone (Fig. 6 A) or with momentum-transfer tube (Fig. 6 B) is not able to simultaneously disperse gas and suck in the gas stream. This can be achieved, however, with the ejector jet nozzle (Fig. 6 C), the ejector (Fig. 6 D), and the Venturi tube (Fig. 6 E). In nozzle selection the ratio of the gas – liquid volumetric flow rates must always be considered. Common values lie between 0.5 and 2. However, much higher values can be achieved in special cases with momentum-transfer tubes [12].

2.3. Flow Regimes

The upward motion of bubbles gives rise to three distinct flow regimes. The crucial quantity for a flow regime is the superficial gas velocity. The *homogeneous flow regime* is marked by a narrow bubble-size distribution, and bubbles are distributed relatively uniformly over the cross section of the apparatus. This regime extends to superficial gas velocities of 0.03 – 0.08 m/s, depending on the gas – liquid system and gas sparger type.

The uniform distribution of gas bubbles vanishes at higher gas rates, and a highly turbulent flow structure appears. In this *heterogeneous* or *churn-turbulent flow regime*, large bubbles or agglomerates of bubbles form and travel upward at high velocity (see Section 2.6), mainly in the axis of the column. The circulating flow that results may be so vigorous that bubbles of a size corresponding to that in the homogeneous regime are actually transported downward in the zone near the column wall (see Section 2.4).

In the small-diameter columns often used as laboratory equipment, *slug flow* occurs at high gas flow rates. Large bubbles are stabilized by the column wall and take on the characteristic slug shape.

The relationship between superficial gas velocity and reactor diameter is illustrated by the flow map of Figure 7 [14]. The broad transition regions are due to the effects of the gas distributor, the gas – liquid system, and the liquid rate. A knowledge of the flow regime is particularly important because it strongly affects the productivity of bubble- column reactors.

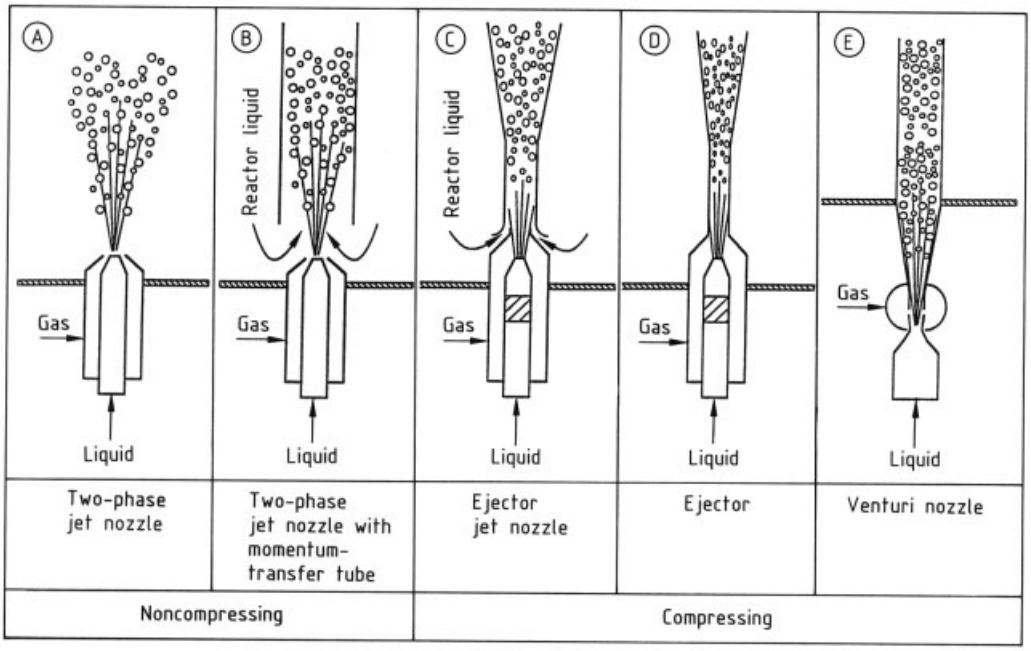

Figure 6. Dynamic gas spargers

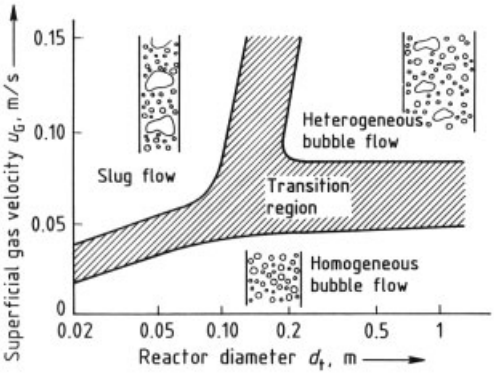

Figure 7. Flow regimes in bubble columns

2.4. Fluid Dynamics

Rising gas bubbles entrain liquid in their wakes. As a rule, this upward flow of liquid is much greater than the net liquid flow rate. Because of continuity, regions therefore exist in which the liquid is predominantly moving downward.

Many theoretical and experimental studies have described the flow behavior of the liquid phase [15]. The circulation velocity is given as a function of superficial gas velocity, column diameter, gas holdup, bubble diameter and rise velocity, viscosity of the liquid, and dispersion height. Published analyses deal with both laminar liquid circulation, which is only of theoretical interest [16–18], and turbulent flow, to which the following discussion is devoted. For example, MIYAUCHI and coworkers use a *force balance* over an annular, axially symmetrical volume element to obtain the velocity profile shown in Figure 8, [19]. Calculation of the velocities, however, requires knowledge of the gas holdup as a function of radial position.

Models of circulation velocity based on *energy balances*, in contrast, assume a cell structure in the bubble column similar to that shown in Figure 9 [20], [21]. In slender bubble columns, both calculations and experimental results show that the height of the circulation cells h_c is equal to the apparatus diameter d_t [20], [22]. JOSHI and SHARMA take into account the energy input due to gas compression and energy losses by dissipation in the wakes of the rising bubbles, as well as liquid transport across the liquid surface (hydraulic pump), thus obtaining a velocity profile over the cross section. HILLS [23] and KOJIMA and coworkers [24] have determined velocity profiles experimentally in bubble columns

having diameters of 0.14 and 5.5 m, respectively (Fig. 10). For the mean circulation velocity $\bar{v}_{\mathrm{L,c}}$ in bubble columns with additional liquid rate u_{L}, JOSHI and SHARMA [20] give the expression

$$\bar{v}_{\mathrm{L,c}} = 1.4 \sqrt[3]{g d_{\mathrm{t}} \left(u_{\mathrm{G}} \pm \frac{\varepsilon_{\mathrm{G}} u_{\mathrm{L}}}{1-\varepsilon_{\mathrm{G}}} - \varepsilon_{\mathrm{G}} v_{\mathrm{rG}} \right)} \qquad (2.1)$$

where ε_{G} is the gas holdup (+ for countercurrent, − for cocurrent). ZEHNER, using a force balance, arrives at a similar relation for the mean circulation velocity [21]:

$$\bar{v}_{\mathrm{L,c}} = \sqrt[3]{\frac{1}{2.5} \cdot \frac{\Delta\varrho}{\varrho_{\mathrm{L}}} g d_{\mathrm{t}} u_{\mathrm{G}}} \qquad (2.2)$$

The velocity profiles derived from the models and, in particular, the mean velocities enable calculation of the essential fluid-dynamic parameters in bubble columns [20], [21], [25].

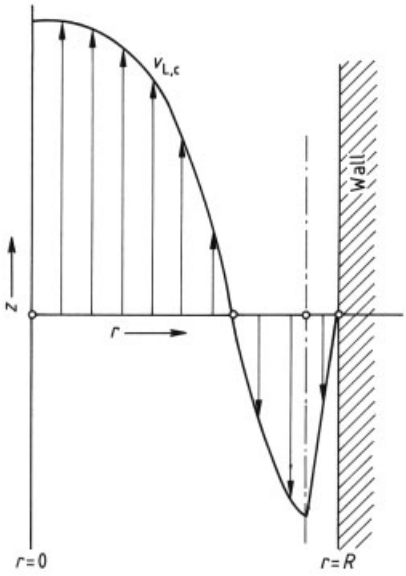

Figure 8. Radial distribution of liquid velocity in a bubble column

2.5. Bubble Size

Analysis of bubble size in bubble columns must distinguish between bubble-size distribution just after bubble formation at the sparger and size distribution further away from the distributor. Because of breakup and coalescence of the rising bubbles, the two distributions can differ significantly. Since the efficiency of bubble columns depends chiefly on bubbles far from the gas distributor,the following discussion only concerns these.

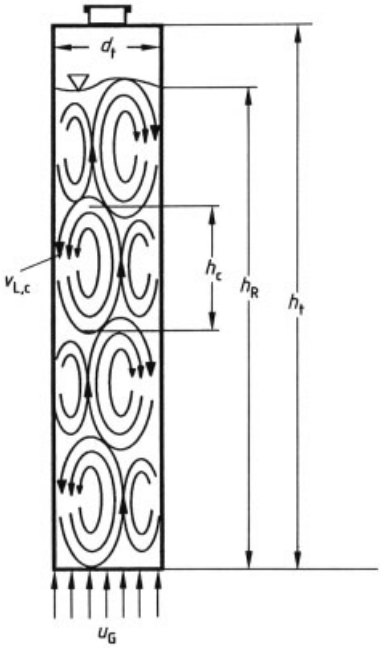

Figure 9. Cell structure in bubble columns

Two basic methods – photography and probe techniques – exist for determining bubble size; however, they do not lead to identical results. Both methods are subject to certain limitations in view of the marked bubble selection that may occur (i.e., not all bubble sizes can be detected) [26], [27]. In particular, any measurement method only leads to realistic results if the flow is homogeneous (i.e., a narrow bubble-size distribution is found). As yet, no method can be recommended for the measurement of large bubbles in the heterogeneous flow regime.

If bubbles are generated in a region of high turbulence (as with *dynamic gas spargers*), the following formula [28] can be used to describe the Sauter diameter d_{bS} (mean bubble diameter, calculated from the volume to surface ratio) [29], [30].

$$d_{\mathrm{bS}} = \frac{2}{e_{\mathrm{M}}^{0.4}} \left(\frac{\sigma}{\varrho_{\mathrm{L}}} \right)^{0.6} \varepsilon_{\mathrm{G}}^{0.5} \left(\frac{\eta_{\mathrm{G}}}{\eta_{\mathrm{L}}} \right)^{0.25} \qquad (2.3)$$

This formula is based on Kolmogorov's theory of isotropic turbulence.

When *static gas spargers* are used, the bubble diameter is only weakly dependent on gas velocity. Descriptive correlations [31–34] are applicable only to the systems and sparger geometries for which they were obtained; a generally valid description of bubble size does not yet exist. The maximum bubble diameter $d_{\mathrm{b,\,max}}$ can be used for purposes of estimation [27], [35]. For low-viscosity liquids, the maximum bubble diameter is given by

$$d_{\mathrm{b,max}} = \sqrt[3]{\frac{\sigma}{g\varrho_{\mathrm{L}}}} \tag{2.4}$$

where σ is the surface tension. For the water – air system, $d_{\mathrm{b,\,max}} = 8$ mm. Larger bubbles have a high probability of being unstable and thus breaking up. The Sauter diameter for real distributions is between 40 and 60 % of the largest stable bubble diameter. This estimate is not, however, applicable to the heterogeneous flow regime due to the binodal bubble-size distribution in this regime.

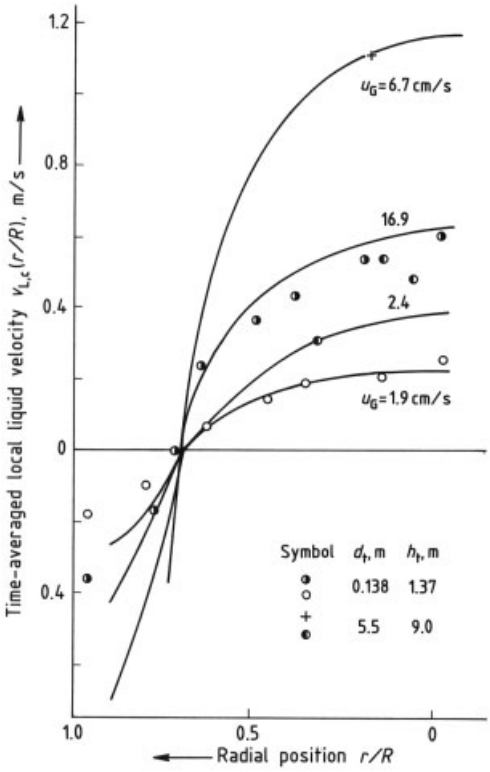

Figure 10. Calculated radial profiles of liquid velocity in bubble columns [20]

2.6. Bubble Rise Velocity

In the homogeneous flow regime, bubbles of almost uniform size and shape rise in the form of a swarm distributed uniformly over the column cross section. When the regime changes, larger bubbles or agglomerates of bubbles form in addition to the bubbles already present [36], [37]. These aggregates rise at a markedly higher velocity than the small bubbles. Figure 11 shows measured velocities for large and small bubbles [36]. Large bubbles first appear at a superficial gas velocity of ca. 0.03 m/s. The formation of large bubbles, however, depends strongly on the type of sparger used. With sintered plates, for example, larger bubbles do not appear at gas rates lower than ca. 0.1 m/s. As shown in Figure 11, large bubbles have a rise velocity that is four or more times larger than small ones. Thus, most of the gas transport in the heterogeneous flow regime is accomplished by large bubbles. In this regime, the quantity of gas transported by small bubbles remains constant, whereas the quantity transported by large bubbles increases linearly with gas velocity. This relationship applies to coalescing and coalescence-hindered gas – liquid systems.

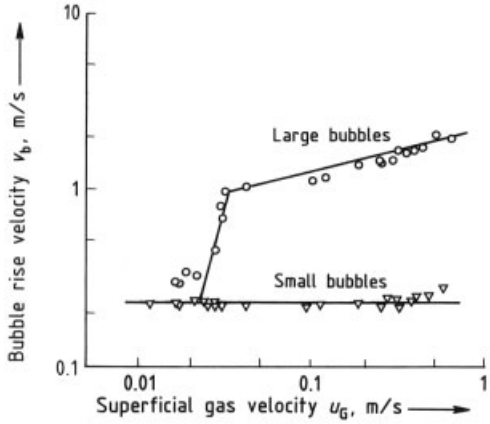

Figure 11. Velocities of rising bubbles for the system water – air
Reactor: $d_t = 0.44$ m, $h_t = 5$ m; Gas distributor: perforated plate ($d_h = 3$ mm)

2.7. Dispersion of the Liquid Phase

Because of the large-scale circulation flows, back-mixing occurs in both phases. The resulting dispersion flow J_{D} is usually governed by an

equation analogous to Fick's first law for molecular diffusion. For the one-dimensional case of axial dispersion, which is generally sufficient for a description, follows

$$J_{\mathrm{D}} = -D_{\mathrm{L}} \frac{\mathrm{d}c}{\mathrm{d}z} \tag{2.5}$$

The dispersion coefficient D_{L} is essentially a function of the superficial gas velocity and the column diameter (e.g., see [38]). Flow direction or liquid velocity does not show any effect, provided the superficial liquid velocity remains within the range common in industry ($u_{\mathrm{L}} < 0.03$ m/s). The dispersion coefficient can be estimated fairly accurately on the basis of fluid-dynamic models. For example, JOSHI and SHARMA [20] and ZEHNER [21] give dispersion coefficients derived from the mean circulation velocity. Each of these formulas gives a good description of the experimentally determined dispersion coefficients known from the literature. By way of example, Figure 12 compares experimental results reported by various workers with the theoretical relation derived by ZEHNER:

$$D_{\mathrm{L}} = \frac{d_{\mathrm{t}} \bar{v}_{\mathrm{L,c}}}{2} = \frac{d_{\mathrm{t}}}{2} \sqrt[3]{\frac{1}{2.5} \cdot \frac{\Delta\varrho}{\varrho_{\mathrm{L}}} g d_{\mathrm{t}} u_{\mathrm{G}}} \tag{2.6}$$

The equation emphasizes that D_{L} strongly depends on column diameter.

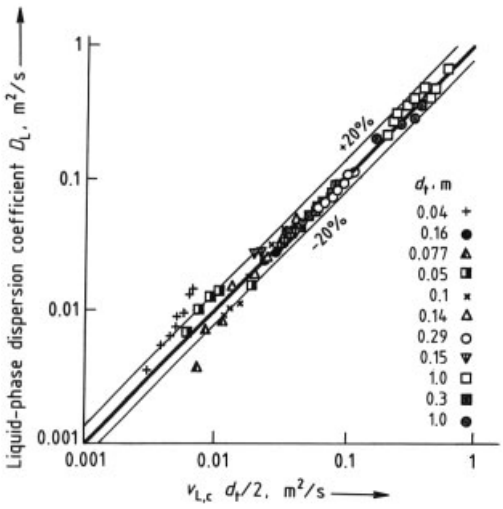

Figure 12. Liquid-phase dispersion coefficient measured by various authors [39]

2.8. Dispersion of the Gas Phase

Due to the large-scale circulation flow both the liquid and gas phases are dispersed. Furthermore, the formation of large and small bubbles, coalescence, and breakup result in additional dispersion in the gas phase. Whereas the gas phase in a bubble column with a smaller diameter flows with virtually no back-mixing, large units behave more like stirred tanks. The gas-phase dispersion coefficient depends more strongly on gas velocity and column diameter than does that of the liquid phase. For this reason, the degree of axial gas mixing is especially relevant for scale-up when the gas phase is expected to show strong concentration variations.

Many formulas in the literature describe the dispersion coefficient as a function of different independent variables. A particularly suitable formula is [40]:

$$D_{\mathrm{G}} = 5 \times 10^{-4} \left(\frac{u_{\mathrm{G}}}{\varepsilon_{\mathrm{G}}} \right)^3 d_{\mathrm{t}}^{1.5} \tag{2.7}$$

This formula is not, however, dimensionally homogeneous (D_{G} in cm^2/s, u_{G} in cm/s, d_{t} in cm), and the gas holdup must be known. By contrast, the equation

$$\varepsilon_{\mathrm{G}} D_{\mathrm{G}} = 0.2 d_{\mathrm{t}} u_{\mathrm{G}} \frac{\frac{\Delta\varrho}{\varrho_{\mathrm{L}}} g d_{\mathrm{t}} u_{\mathrm{G}}}{v_{\mathrm{rG}}^3} \tag{2.8}$$

derived by ZEHNER and SCHUCH is dimensionally correct [41]. However, more recent measurements [42] have shown that this correlation must be modified in the heterogeneous flow regime ($u_{\mathrm{G}} \geq 5$ cm/s) because the proportionality is somewhat different:

$$\varepsilon_{\mathrm{G}} D_{\mathrm{G}} \sim (u_{\mathrm{G}} d_{\mathrm{t}})^{1.65}$$

2.9. Gas Holdup

Gas holdup is one of the most important operating parameters because it not only governs phase fraction and gas-phase residence time but is also crucial for mass transfer between liquid and gas. Gas holdup depends chiefly on gas flow rate, but also to a great extent on the gas – liquid system involved. Accordingly, many correlations that

have been published only apply to the systems investigated.

Gas holdup is defined as the volume of the gas phase divided by the total volume of the dispersion:

$$\varepsilon_G = \frac{V_G}{V_G + V_L} \tag{2.9}$$

The relationship between gas holdup and gas velocity is generally described by the proportionality

$$\varepsilon_G \sim u_G^n$$

In the homogeneous flow regime, n is close to unity. When large bubbles are present, the exponent decreases, i.e., the gas holdup increases less than proportionally to the gas flow rate (Fig. 13). The higher the contribution of large bubbles to the total gas holdup, the smaller is the exponent n. In the fully developed heterogeneous flow regime, n finally takes on values between 0.4 and 0.7, depending on the gas – liquid system.

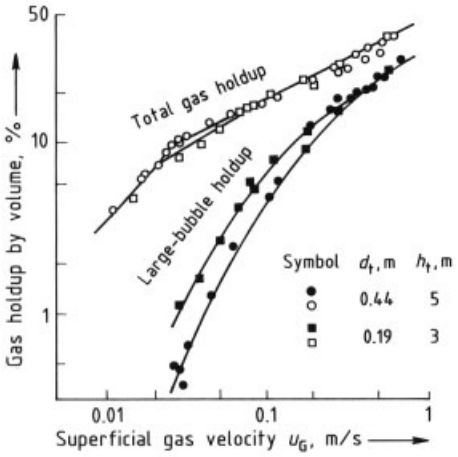

Figure 13. Gas holdup and fraction of large bubbles (system: water – air; gas distributor: perforated plate $d_h = 3$ mm)

The effect of low *liquid velocities* u_L on gas content is generally negligible. At high flow rates the gas holdup decreases in cocurrent systems because gas bubbles pass through the column more quickly. In contrast, the gas holdup rises in countercurrent systems; this can lead to extremely high gas holdup, especially in downflow bubble columns [43].

Above 0.1 m, the reactor diameter is of secondary importance for gas holdup, as measurements on units having diameters between 0.1 and 5.50 m show [34], [36], [44], [45].

The effects of *physical properties* on gas holdup are exceedingly complex. Increasing the viscosity of the liquid phase leads to increased bubble coalescence and thus a decrease in gas holdup. Above ca. 50 mPa · s, however, the gas holdup remains constant [46]. Although surface tension is not very important for the gas holdup, a change in coalescence behavior may have lasting effects. When gas-phase residence times are long and gas distribution is obtained with perforated or sintered plates, the presence of salts or alcohols that counteract coalescence has little effect [44]. In contrast, gas holdup increases markedly in systems sparged by two-phase nozzles when coalescence is hindered [47]. Such behavior can be attributed to a small-bubble gas holdup higher than that in coalescing systems, whereas the content of large bubbles is identical [36]. Small bubbles formed under high shear stresses in the region near the two-phase nozzle cannot recombine so the gas holdup increases significantly with this type of gas distributor.

The relation of Akita and Yoshida [48] is suitable for estimating the gas holdup and is based on the investigation of numerous systems:

$$\frac{\varepsilon_G}{(1-\varepsilon_G)^4} c_1 = \left(\frac{g d_t^2 \varrho_L}{\sigma}\right)^{\frac{1}{8}} \left(\frac{g d_t^3}{\nu_L}\right)^{\frac{1}{12}} \left(\frac{u_G}{\sqrt{g d_t}}\right) \tag{2.10}$$

For pure liquids and nonpolar solutions the constant c_1 is 0.2, for electrolyte solutions it is 0.25. However, reliable results cannot be expected for systems that have not been investigated in this study. The effects of *reactor pressure* on gas holdup have not been fully explained. Although some authors find no effect between 1 and 16 bar [49], others find that gas holdup increases with pressure in systems with small sparging holes ($d_h \leq 1$ mm) or with sintered plates [44], [50–52]. Transition from the homogeneous to the heterogeneous regime occurs at higher gas flow rates as pressure increases.

Gas holdup is generally a function of position in the bubble column. Axial profiles of gas holdup show a zone near the gas distributor in which the holdup increases to the value that characterizes the following equilibrium zone. The gas holdup at the top of the column, in the zone

of bubble breakup, is markedly higher than the equilibrium value [45].

Gas holdup also depends on radial position. The profile shows gradients only near the wall in the homogeneous flow regime [23], [45], [53]. In contrast, a parabolic radial gas holdup distribution appears in the heterogeneous regime [23], [37], [45], as a consequence of the preferential rising of large bubbles or agglomerates of bubbles in the axis of the column. Figure 14 shows radial profiles of gas holdup at various gas flow rates in the water – air system.

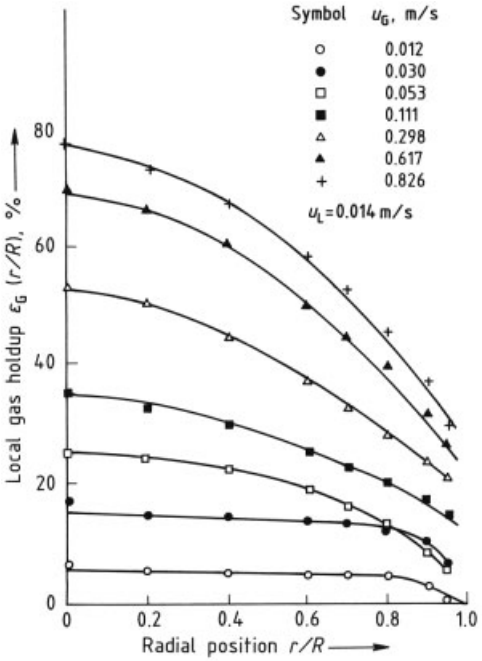

Figure 14. Radial profiles of local gas holdup
d_t = 0.45 m; h_t = 6.2 m; h = 3.03 m (at measurement point); perforated plate d_h = 1 mm

2.10. Specific Interfacial Area

The area of the gas – liquid interface is one of the most important process parameters. Especially at high reaction rates (e.g., when a bubble column is employed as an absorber), the interfacial area becomes a crucial factor in equipment sizing. Like gas holdup, interfacial area depends on the geometry, operating conditions, and gas – liquid system. Gas holdup and interfacial area per unit volume are related as

$$a = \frac{A}{V_R} = \frac{6\varepsilon_G}{d_{bS}} \tag{2.11}$$

where V_R is the volume of the reaction mixture and d_{bS} is the mean bubble diameter (Sauter diameter, Section 2.5). As Figure 15 shows, the interfacial area increases with increasing gas flow rate. An exception occurs when a porous-plate sparger is used; like gas holdup, interfacial area decreases on transition to the heterogeneous flow regime and then approaches the same values observed with perforated plates. The growth in interfacial area with increasing gas velocity is always greater in the homogeneous than in the heterogeneous flow regime. The reason lies in the formation of large bubbles in the heterogeneous regime: the interfacial area of large bubbles per unit volume is markedly lower than that of smaller ones.

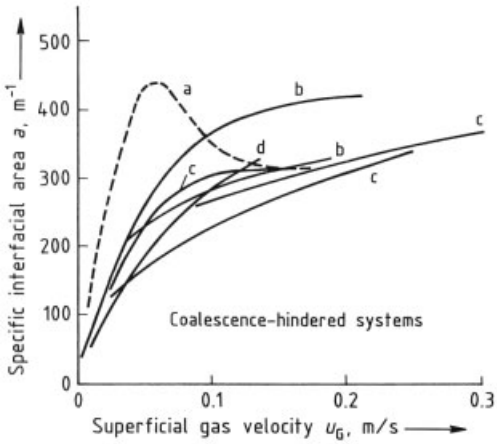

Figure 15. Specific interfacial area as a function of superficial gas velocity
a) d_t = 0.102 m; b) d_t = 0.29 m; c) d_t = 0.14 m; d) d_t = 0.1 m; – – Porous plate; —- Perforated plate

The specific interfacial areas attainable in various gas – liquid reactors can be compared on the basis of power input P per unit volume [29]. Experimental values can be described by the relation

$$a = k\left(\frac{P}{V_R}\right)^m \varepsilon_G^n \tag{2.12}$$

The exponent m is between 0.4 and 1 [54]. The plot in Figure 16 enables a direct comparison to be made between reactors with respect to the energy required to produce a given interfacial area.

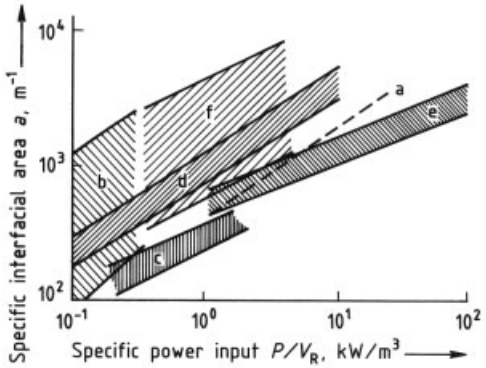

Figure 16. Specific interfacial area as a function of specific power input [55]
a) Stirred tank; b) Bubble column with porous plate; c) Bubble column; d) Bubble column with two-phase jet nozzle (jet loop reactor); e) Packed column; f) Bubble column with injector nozzle

2.11. Volumetric Mass-Transfer Coefficient

The mass transfer between the gas and the liquid phase in a bubble column can be described in most cases by the volumetric mass-transfer coefficient $k_L a$, which is the liquid-phase masstransfer coefficient k_L multiplied by the specific interfacial area. Gas-phase resistance can usually be neglected, so $k_L a$ gives an adequate description. To determine the mass-transfer rate, however, the driving concentration difference must be known which in turn requires a knowledge of mixing behavior in the gas and the liquid phase. In industrial units ($d_t > 1$ m), estimates can be based on the assumption of complete mixing in both liquid and gas phases.

Like gas holdup and interfacial area, $k_L a$ also depends on the gas flow rate, type of sparger, and gas – liquid system. The mass-transfer coefficient and the gas rate are again proportional to one another:

$$k_L a \sim u_G^n$$

where n can be between 0.7 and 0.92 [31], [56–59]. Mass-transfer coefficients two- to threefold higher can be achieved in the homogeneous flow regime if a porous plate is used as sparger instead of a perforated plate (Fig. 17). In the heterogeneous regime, however, the effect of the sparger is negligible.

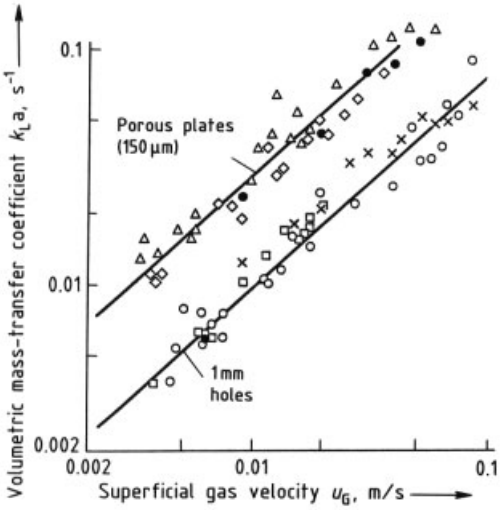

Gas distributor	d_t, m	h_t, m	Flow direction	Symbol
Cross sparger	0.20	0.250	↑↑	×
		0.723	↑↑	○
		0.723	↑↓	□
Porous plate	0.10	0.250	↑↑	●
	0.15	0.440	↑↑	△
	0.15	0.440	↑↓	◇

Figure 17. Mass-transfer coefficients in bubble columns

According to experimental results, the column diameter above about 15 cm has no effect on mass-transfer coefficient. Some correlations nonetheless include reactor diameter [31], [57], [60]. AKITA and JOSHIDA [31] state that the value of the column diameter used for calculation should not be increased beyond 0.6 m. Based on this premise, their correlation for $k_L a$ is

$$\frac{k_L a d_t^2}{D_{G,L}} = 0.6 \left(\frac{\nu_L}{D_{G,L}}\right)^{0.5} \left(\frac{g d_t^2 \varrho_L}{\sigma}\right)^{0.62} \left(\frac{g d_t^3}{\nu_L^2}\right)^{0.31} \varepsilon_G^{1.1} \quad (2.13)$$

and has the best experimental support. The mass-transfer coefficient increases in coalescence-hindered systems [54], [61]. This increase depends on the system and the concentration of coalescence-hindering substance. The maximum gain in mass-transfer coefficient due to the presence of electrolytes, however, is only 30 %.

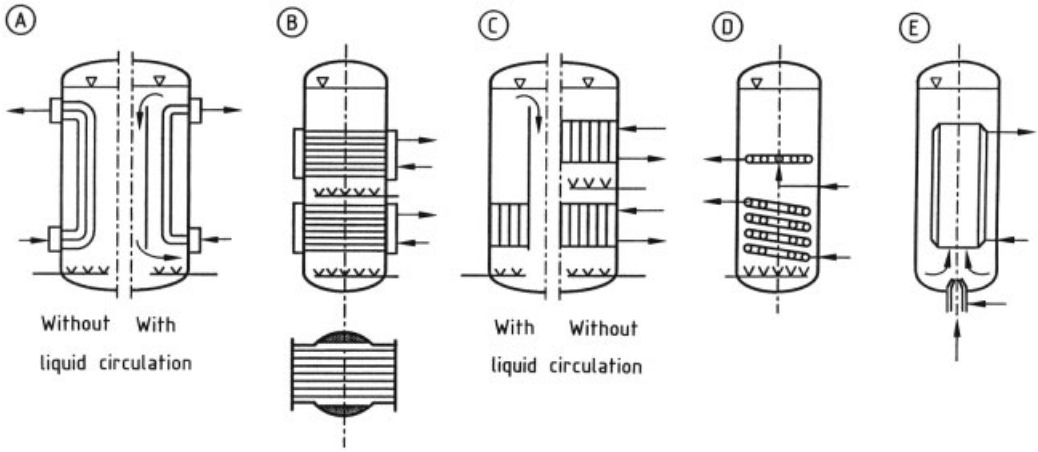

Figure 18. Examples of heat exchanger inserts
A) Parallel single tubes; B) Tube bundle in cross flow; C) Longitudinal tube bundle; D) Tube spiral or helix; E) Draft tube with jacket

2.12. Heat Transfer

In many cases, heat must be removed when operating bubble columns. A particularly simple solution is to utilize the latent heat of vaporization of the liquid phase for heat removal, although this is not always feasible. In addition, many possibilities exist for heat transfer through heated or cooled surfaces, as shown in Figure 18. In this way, up to ca. 30 m^2/m^3 of heat-transfer area can be installed in a bubble column.

The turbulent flow generated by rising gas bubbles increases heat transfer even at low gas rates (Fig. 19). The increase in heat-transfer coefficient α, with gas throughput is markedly greater in the homogeneous than in the heterogeneous regime.

The heat-transfer coefficient does not depend on the column diameter, type of sparger, or coalescence behavior of the gas – liquid system.

Two distinct concepts are used to describe the heat-transfer coefficient at the wall. Whereas KAST [62] and DECKWER [63] consider radial flow and heat transported by it, JOSHI and coworkers [64] and ZEHNER [21] use circulation velocities derived by them for physical modeling. Here with the following relation for the heat-transfer coefficient α can be derived [21]:

$$\alpha = 0.18\,(1-\varepsilon_G)\left(\lambda_L^2 \varrho_L c_{pL} \cdot \frac{\bar{v}_{L,c}^2}{l \cdot \nu_L}\right)^{1/2} \qquad (2.14)$$

where

$$l = d_b \left(\frac{\pi}{6\varepsilon_G}\right)^{1/3}$$

and $\bar{v}_{L,c}$ is calculated by Equation (2.2). On the whole, these two approaches correlate well with literature data. Heat transfer in bubble columns with heat-exchange internals has not been intensively studied [65–69]. For tube bundles arranged in an axial direction (Fig. 18 C), the heat-transfer coefficient increases with increasing tube pitch and decreases when the free cross-sectional area increases [68], [69]. A similar relationship is found for a tube bundle arranged in cross flow (Fig. 18 B), but here a marked effect of liquid throughput occurs [67].

The installation of tube bundles leads to an overall change in fluid dynamics and thus in mixing behavior. For example, tubes installed in cross flow hinder flow in the longitudinal direction and thus reduce dispersion in the liquid phase [70]. In contrast, the arrangement of heat-transfer surfaces in the flow direction leads to more intense mixing of the liquid phase by intensifying circulation [71], [72].

2.13. Slurry Bubble Columns

Solid particles are present in bubble columns in a wide variety of processes; they must be held

in suspension by the rapid liquid circulation already discussed. The presence of the solid phase in a slurry bubble column means that all process parameters behave differently, and in a more complicated way, than in a two-phase bubble column.

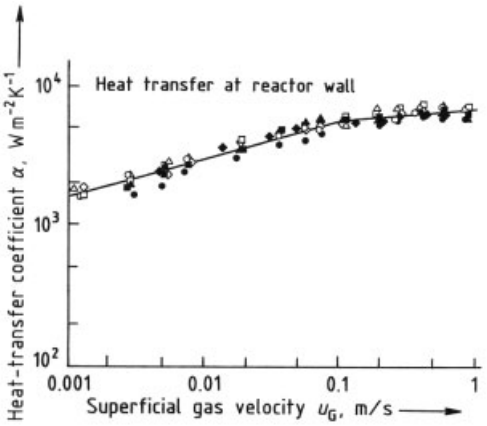

Symbol	Distributor	d_h, mm	System
○	porous plate	0.02	water – air
△	porous plate	0.15	
◇	perforated plate	1.00	
□	perforated plate	2.00	
●	porous plate	0.02	NaCl solution – air
▲	porous plate	0.15	
◆	perforated plate	1.00	
■	perforated plate	2.00	

Figure 19. Heat-transfer coefficient at reactor wall $d_t = 0.196$ m; $h_t = 6.20$ m; liquid velocity $u_L = 1.2$ cm/s

The *minimum gas velocity* necessary to hold the solids in suspension increases as the concentration and density of the particles increase. The increment depends, however, on the physical properties of the solid and liquid phases. Many empirical equations for the critical gas velocity for complete suspension show a marked increase with increasing single-particle settling velocity. Equation (2.15) [73] can be used for design purposes:

$$\frac{u_{G,\min}}{v_{rS}} = 0.801 \left(\frac{\varrho_S - \varrho_L}{\varrho_L}\right)^{0.6} \left(\frac{\bar{\varphi}_S}{\varrho_S}\right)^{0.146} \left(\frac{\sqrt{g d_t}}{v_{rS}}\right)^{0.24} \left[1 + 807 \left(\frac{g \eta_L^4}{\varrho_L \sigma^3}\right)^{0.578}\right] \quad (2.15)$$

where v_{rS} is the relative settling velocity of the particle swarm in the liquid. At low solids concentration (< 10 wt %) and low settling velocity of the particles the *gas holdup* is nearly unchanged [74]. In contrast, the gas holdup decreases at higher settling velocities with increasing solids concentration [75–77]. The strength of this effect differs from one flow regime to another. The decrease is particularly marked when an increase in solids content leads to a change from the homogeneous to the heterogeneous regime. On the other hand, in the heterogeneous regime the reduction in gas holdup is only slight with increasing solids content. YASUNISHI and coworkers [78] verify and recommend the gas holdup relation of KOIDE and coworkers [79]

$$\frac{\varepsilon_G}{(1-\varepsilon_G)^4} = \frac{0.277 \left(\frac{u_G \eta_L}{\sigma}\right)^{0.918} \left(\frac{g \eta_L^4}{\varrho_L \sigma^3}\right)^{-0.252}}{1 + 4.35 \left(\frac{\bar{\varphi}_S}{\varrho_S}\right)^{0.748} \left(\frac{\varrho_S - \varrho_L}{\varrho_L}\right)^{0.881} \left(\frac{d_t u_G \varrho_L}{\eta_L}\right)^{-0.168}} \quad (2.16)$$

for a wide range of solids concentrations and liquid properties. For coalescence-hindered aqueous electrolyte solutions a coefficient 0.364 must be used instead of 0.277 in Equation (2.16). The *mixing behavior* of the liquid and the gas phase is very similar to that in the two-phase bubble column. The axial solids distribution can be described by a one-dimensional sedimentation – dispersion model. The *solids dispersion coefficient* is generally lower than the corresponding liquid dispersion coefficient [80]. The difference between the two values increases rapidly with increasing settling velocity of particles. For small solid particles ($v_{rS} < 0.01$ m/s), the effect of superficial gas velocity on the axial solids concentration profile is negligible above the minimum gas velocity for suspension [81].

The *specific interfacial area* declines continuously with increasing solids content [76], [82]. This phenomenon can be explained by the formation of larger gas bubbles, due to the presence of solid particles that lead to the observed decrease in gas holdup. If, however, very fine particles are used in aqueous electrolyte solutions (i.e., systems with hindered coalescence), the interfacial areas produced do not differ from those in the two-phase system [83].

The effect of solids on the *volumetric mass-transfer coefficient* depends largely on particle properties, solids content, and physical properties of the liquid. At low solids concentration (up

to ca. 3 – 5 wt %), the mass-transfer coefficient matches that of the two-phase bubble column. A higher solids content, like increasing particle size, leads to a drop in $k_L a$ relative to the solid-free condition [78], [79], [84], [85]. For very fine particles ($d_P < 36\,\mu m$), however, $k_L a$ also decreases with decreasing particle diameter [86]. Overall, the behavior of $k_L a$ is governed by the interfacial area per unit volume because the change in k_L is generally small.

The mass-transfer coefficient between *liquid and solid* increases roughly as the fourth root of the gas flow rate, decreases with increasing liquid viscosity and particle diameter, and becomes partly independent of these factors at high gas rates. Two distinct models can be used for the mathematical description, but they lead to similar values if the solids are completely suspended. Values reported by various authors are compared in Figure 20 [87].

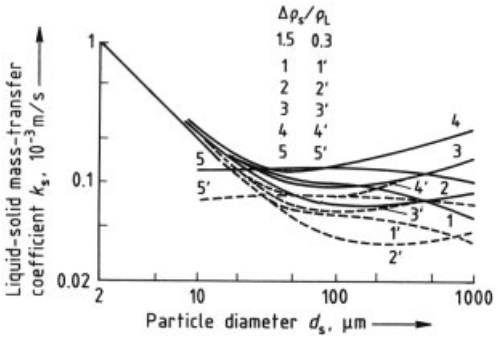

Figure 20. Liquid – solid mass-transfer coefficient estimated with five different correlations [87]
$\nu_L = 10^{-6}\,m^2/s$; $\varrho_L = 1000\,kg/m^3$; $D_{G,L} = 10^{-9}\,m^2/s$;
—· $\Delta\varrho_S/\varrho_L = 1.5$; – – – $\Delta\varrho_S/\varrho_L = 0.3$

Hydrogenation of Benzene. In the IFP process, benzene is hydrogenated to cyclohexane in a slurry bubble column [88] (→ Cyclohexane, Chap. 4.1.). This process was used to produce 1.8×10^6 t of cyclohexane in 23 plants worldwide in 1991.

Figure 21 shows the slurry bubble column (a) in which benzene is hydrogenated on suspended Raney nickel. The hydrogen-rich gas that is let in at the bottom of the main reactor provides hydrogen for the reaction and also strips the product cyclohexane out of the reactor. Thus, the process can be operated without the need for expensive equipment to separate the product from the catalyst. In the external cooling loop, the high heat of reaction is removed and suspension of the solid catalyst is assisted by the circulating liquid stream. Complete conversion of benzene is accomplished in a fixed-bed reactor (b) installed downstream on the gas side.

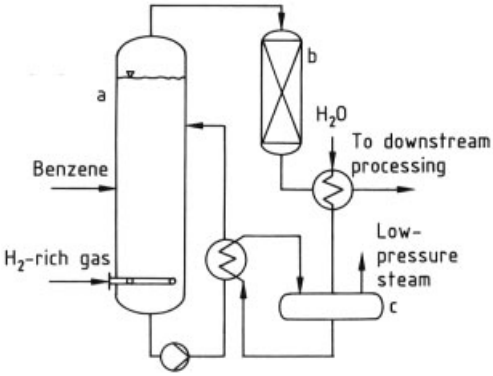

Figure 21. Hydrogenation of benzene to cyclohexane
a) Main reactor; b) Secondary reactor; c) Steam drum $h_t = 10$ m; $d_t = 2.5$ m; $T = 195\,°C$; $p = 22$ bar; Gas velocity: 7.5 cm/s; Liquid residence time ~ 3 h

The usual reaction conditions in the bubble-column reactor are 200 °C and 22 bar. Typical gas velocities are ca. 0.08 m/s; liquid-phase residence time is ca. 3 h.

2.14. Airlift Loop Reactors

In contrast to bubble columns, airlift loop reactors are characterized by a well-defined liquid circulation, which is achieved by dividing the reactor into sections with and without gas sparging. The difference in gas holdup between these two zones drives the liquid circulation. In principle, two types of airlift loops can be identified (Fig. 22). In the first (airlift reactors with internal loop), either a concentric tube (Fig. 22 A, B) or a plane partition (Fig. 22 C) divides the column into riser and downcomer sections. In the second (airlift reactors with external loop, Fig. 22 D), two separate tubes form the upflow and downflow zones; the tubes are joined by two horizontal sections at top and bottom.

The dependence of liquid circulation velocity on superficial gas velocity is described by the purely empirical relation

$$\bar{v}_{L,c} = C_1 u_G^{C_2} \qquad (2.17)$$

The value of the constant C_1 is determined by reactor geometry and the physical properties of the system; C_2 depends on both flow regime and reactor geometry [89–91]. A physical model based on an energy balance [39], [92] leads to the relation

$$\bar{v}_{L,c} = c \cdot \sqrt[3]{g h_R u_G} \tag{2.18}$$

An exponent of 0.33 for gas flow rate is of the order of usual experimental results.

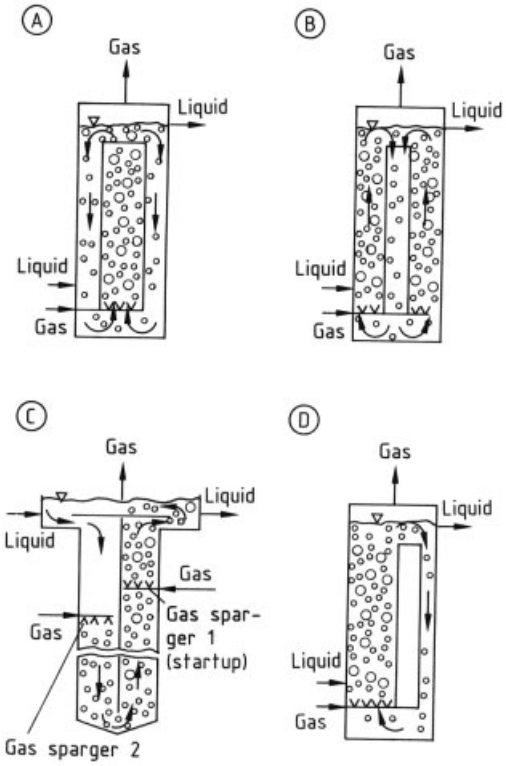

Figure 22. Types of airlift loop reactors
A) Concentric draft tube with external recycle; B) Concentric draft tube with internal recycle; C) Deep shaft reactor (ICI); D) External loop

Airlift reactors with external loop (Fig. 22 D) are usually run at much higher gas and liquid flow rates than conventional bubble columns. The high circulation velocities significantly change the nature of the two-phase flow, namely, the gas holdup declines with increasing circulation velocity (see Fig. 23). The highest gas holdup occurs in the bubble column ($u_L = 0$), where the absolute velocity of the rising bubbles is lowest because of the zero liquid velocity. Parameters such as surface tension, coalescence, and viscosity have much less effect on airlift loop reactors than on bubble columns because the interactions between bubbles are far weaker as a result of the high circulation velocity. For the same reason, the homogeneous flow regime in airlift loop devices extends to much higher gas rates than in bubble columns [91], [93].

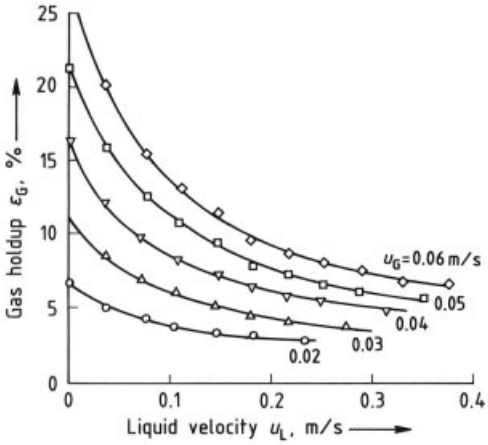

Figure 23. Gas holdup in airlift reactors with external loop (system: 0.1 mol/L NaCl solution – air) $d_t = 0.1$ m; $h_t = 8.5$ m; Porous plate = 150 µm

The gas holdups that occur in *airlift reactors with internal loop* are only slightly lower than those in bubble columns. The decrease in gas holdup in the riser is partly offset by an increase in the downcomer [94], [95].

As in the bubble column, the *volumetric mass-transfer coefficient* increases with increasing gas flow rate. Because the liquid-phase mass-transfer coefficients k_L are the same in bubble columns and airlift reactors [96], [97], the difference in $k_L a$ results from differences in interfacial area. Airlift reactors with external loop always have lower mass-transfer coefficients than bubble columns because the lower gas holdup implies a smaller area for mass transfer. The $k_L a$ values for airlift reactors with internal loop, on the other hand, are similar to the values for bubble columns (Fig. 24) because here the gas holdups differ only slightly [93], [98–100].

In contrast to bubble columns, the residence-time distribution of airlift reactors is influenced not just by longitudinal mixing but also by back-mixing due to the circulation flow. Reactors with an external loop exhibit axial dispersion coefficients whose values are up to 20 % lower than

those of bubble columns, depending on the circulation velocity [93]. The consequences of this back-mixing for the reactor yield of airlift loops, however, are far less serious because the high liquid velocities lead to far larger Bodenstein numbers (for a definition of the Bodenstein number, see → Mathematical Modeling). The axial dispersion coefficients of airlift reactors with internal loop are much lower. Measurements of axial mixing of the gas and liquid phases show a decrease in the dispersion coefficients by roughly a factor of three [101].

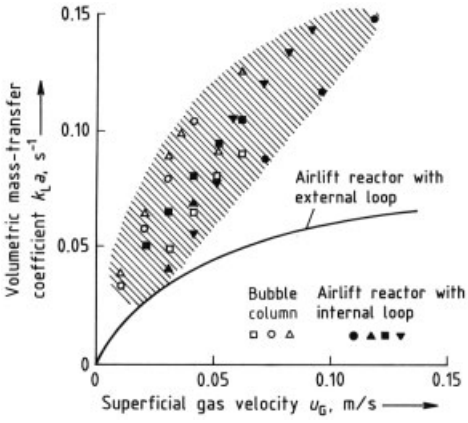

Figure 24. Comparison of mass-transfer coefficients for airlift reactors and bubble columns
(system: salt solutions; gas distribution: small bubbles)

As in bubble columns, mixing times decrease with increasing superficial gas velocity because the circulation velocity becomes greater. Since the circulation time t_c and the mixing time t_M are directly proportional [92]

$$\frac{t_M}{t_c} = \gamma \left(\frac{F_D}{F_R} \right)^{0.5} \tag{2.19}$$

(where $\gamma = 3.5$ for internal circulation and 5.2 for external circulation), the relationship between mixing time and circulation velocity can be expressed as

$$t_M \sim \bar{v}_{L,c}^{-1}$$

The mixing time is also directly proportional to the distance traveled. Five to six passes are required for a degree of mixing of 90 %. The liquid circulation in airlift reactors, with their high circulation velocities, leads to higher heat-transfer coefficients than in bubble columns [102]. As in bubble columns, the heat-transfer coefficient in airlift loop reactors increases with gas flow rate.

Biological Wastewater Treatment. Airlift loops are employed to provide well-defined back-mixing of the liquid phase. This is desirable, for ex-ample, when uniform temperature and concentration distributions must be maintained in the reaction medium to equalize feed variations as quickly as possible or to prevent settling of solids from the mixture.

Airlift reactors are used in biological wastewater treatment [5], [103], [104]. These units are closed vessels ca. 15 – 25 m tall and 10 – 45 m in diameter; they have small space requirements, very good oxygen utilization, and greatly reduced off-gas and noise emissions. The contents of the reactor circulate through one or more draft tubes (Fig. 25); sparging occurs outside the draft tubes. During operation, the growing microorganisms must constantly be provided with sufficient oxygen and substrate, and adequate mixing of the wastewater – activated-sludge mixture must be insured. If these conditions are not satisfied, solids will settle and anaerobic fermentation processes may occur. The usual conditions are as follows: superficial gas velocity 1 – 3 mm/s, gas holdup between 1 and 3 %, and roughly 25 circulations of reactor contents per hour. The utilization of atmospheric oxygen is more than 50 %. The wastewater has a residence time between 6 and 15 h.

3. Downflow Bubble Columns

Chapter 2 described ordinary bubble columns in which gas flows from bottom to top and has a short residence time (gas sparging method A in Fig. 1). In downflow bubble columns, by contrast, the gas and liquid phases are transported together from top to bottom (Fig. 1 B). This regime demands liquid velocities v_L greater than the relative velocity v_{rG} between the two phases. Depending on the liquid velocity chosen, very low gas velocities can be achieved

$$v_G = v_L - v_{rG} \tag{3.1}$$

or long residence times. This is an advantage especially when a large-volume liquid stream must come in contact with a small-volume gas stream. In the extreme case, a virtually suspended state

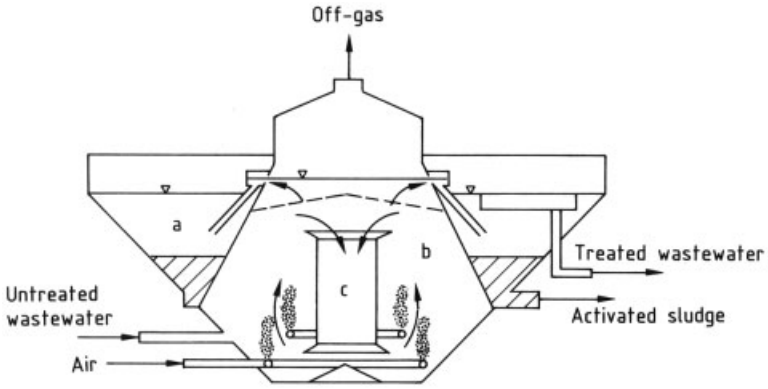

Figure 25. Biohoch reactor (Hoechst)
a) Settling zone; b) Aeration chamber; c) Draft tube

of the bubbles can be realized, with an arbitrarily long residence time. Under certain conditions, this permits complete conversion of the gas. Normally, however, part of the gas must be assumed to exit the reactor without reacting, mainly when the gas contains components that do not react. In such cases, the cocurrent motion of the phases is a disadvantage because only one theoretical transfer unit can be realized.

3.1. Design and Applications

As with bubble columns, a variety of designs exist for downflow bubble columns. These differ mainly in the way the gas is let in, the bubbles are generated, and the unreacted gas is removed. Figure 26 shows some examples.

The *simple downflow bubble column* (Fig. 26 A) is particularly suitable for gases that are soluble in the liquid phase and/or fast reactions. Unreacted gases cannot be separated in the column, so an extra separator may be required. The simple downflow bubble column is often employed at high pressure (> 100 bar). A slender geometry makes it possible to reduce the wall thickness of the cylindrical reactor. To improve mass transfer between gas and liquid phases, the vessel can be packed with particles, which also reduce both the required liquid rate and the axial mixing of liquid and gas. Usually, however, packings are used as catalyst supports. The classical application of this type of device is the hydrogenation of a wide range of substances.

Adding a liquid recycle creates diverse process design options. The back-mixing involved, which is usually undesirable, can often be acceptable. With a liquid recycle the downflow bubble column can be operated on small feedstreams. The recycle loop also provides a simple way of adding or removing heat, so that the temperature profile in the reactor becomes more uniform.

From the standpoint of process engineering, the *downflow bubble column with integrated separator* (Fig. 26 B) differs little from the simple downflow bubble column. The integrated separator is well suited when larger quantities of off-gas must be removed. A typical application is in the ozone treatment of water air or oxygen with a low ozone content is fed to the reactor and the quantity of exit gas is almost the same as the quantity of inlet gas. The design of the reactor with integrated separator is simple. The shouldered form is not suitable for high pressure.

The *downflow – upflowbubble column* (Fig. 26 C) combines a downflow bubble column and an ordinary bubble column. Particularly long gas residence times are possible. The liquid routing shown in Figure 26 C gives a frequently desirable residence-time distribution: the downflow section features mixing similar to a stirred tank by virtue of the pump stream. This is advantageous with a high heat of reaction, which can be removed with the pump stream. The bubble column in the outer annular space merely carries the outflow, and back-mixing in this zone can be suppressed by internals (pack-

ing, static mixers, sieve trays). High conversion are achieved in higher-order reactions.

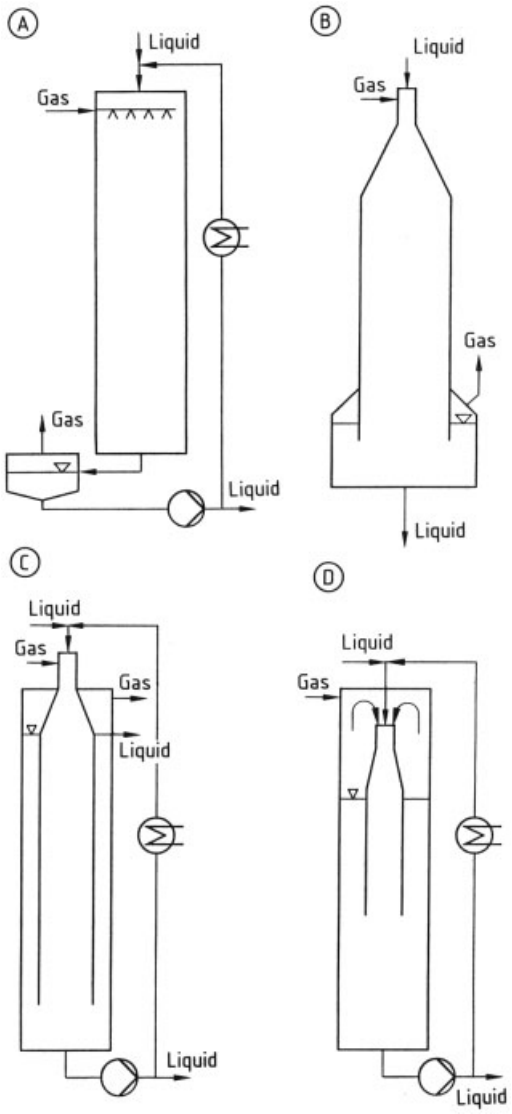

Figure 26. Designs of downflow bubble columns
A) With external gas separator; B) With integrated gas separator; C) Combined downflow – upflow with bubble column in annulus; D) Dip-tube gas sparging with internal gas recycle

Downflow – Upflow Bubble Column (Fig. 26 D). Another design combines downflow and ordinary bubble columns. However, the top of the downflow section is in the gas space of the reactor. Fresh gas together with recycle gas (that has escaped from the liquid surface) is drawn in here and dispersed in the liquid. Pure gases or gases with low inerts content can be completely converted under pressure with this method, also called *dip-tube sparging*.

The lower part of the downflow bubble column serves as the separator. Only small gas bubbles are carried out of the reactor, which still have some reactivity. The pump is therefore protected against excessive contents of gas in the liquid, even in coalescence-hindered systems.

3.2. Operating Conditions and Gas Holdup

Gas is fed in at the top of the column and distributed as uniformly as possible over the cross section. Large gas holdups ($\varepsilon_G \approx 0.3-0.35$) can be obtained even in coalescing systems such as water – air [105–110]. When the system is coalescence-hindered, for example, if carboxymethyl cellulose or ethanol has been added to the water – air system, values up to $\varepsilon_G \approx 0.45$ can be achieved [108].

The gas holdup can be estimated as

$$\varepsilon_G = \frac{u_G}{v_L - v_{rG}} \tag{3.2}$$

The relative velocity v_{rG} for coalescing aqueous systems takes on values in the range $0.2\,\text{m/s} \leq v_{rG} \leq 0.3\,\text{m/s}$. The liquid velocity v_L can be calculated from the liquid rate u_L and the gas holdup ε_G:

$$v_L = \frac{u_L}{1-\varepsilon_G} \tag{3.3}$$

Hence the gas holdup can be expressed as

$$\varepsilon_G = \frac{u_G}{\frac{u_L}{1-\varepsilon_G} - v_{rG}} \tag{3.4}$$

If gas and liquid rates are given, Equation (3.4) can be solved for the gas holdup:

$$\varepsilon_G = \frac{B}{2}\left[+\sqrt{\left(\frac{2}{B}\right)^2 \frac{u_G}{v_{rG}} + 1} - 1\right]$$

where

$$B = \frac{u_L + u_G}{v_{rG}} - 1 \tag{3.5}$$

Finally, Equation (3.4) can be written so as to yield the liquid rate:

$$u_{\mathrm{L}} = (1-\varepsilon_{\mathrm{G}})\left(\frac{u_{\mathrm{G}}}{\varepsilon_{\mathrm{G}}} + v_{\mathrm{rG}}\right) \tag{3.6}$$

A flow chart can then be derived for the water – air system ($v_{\mathrm{rG}} = 0.23$ m/s). In Figure 27, the gas velocity is plotted versus the superficial liquid velocity, with the gas holdup ε_{G} as a parameter. For $\varepsilon_{\mathrm{G}} > 0.35$, flow is in the heterogeneous regime. In this regime a highly turbulent two-phase flow develops, resulting in strong mixing of liquid and gas. In the extreme case, gas accumulates at the top and can propagate throughout the reactor from there. KULKARNI reports somewhat different results [111], possibly because of less uniform gas feeding.

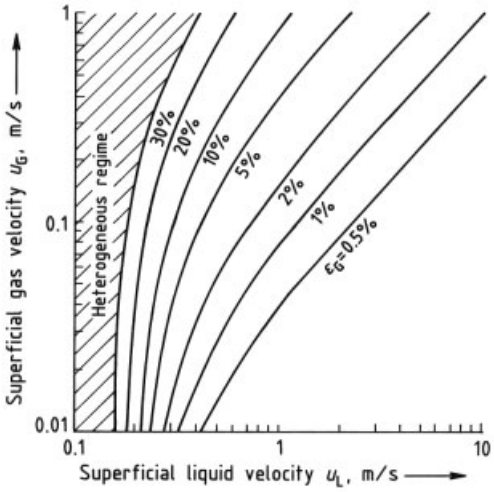

Figure 27. Flow chart for downflow bubble columns
Gas velocity is plotted as a function of liquid velocity, with gas holdup as parameter, for the water – air system ($v_{\mathrm{rG}} = 0.23$ m/s) calculated with Equation (3.6).

For systems with hindered coalescence, determination of these values and other process parameters normally requires experimentation [105].

3.3. Mass Transfer

The following statements are applicable only to coalescing systems. In the homogeneous flow regime, all bubbles in the downflow bubble column are almost equal in size. Diameters of $3\,\mathrm{mm} \leq d_{\mathrm{b}} \leq 4\,\mathrm{mm}$ are observed [112]. A slight decrease in bubble size with increasing liquid flow rate and rising pressure has been reported [108].

If the gas holdup is known, the specific interfacial area can be estimated as

$$a = \frac{6\varepsilon_{\mathrm{G}}}{d_{\mathrm{bS}}}$$

which gives maximum values up to $a = 450 - 700\,\mathrm{m}^{-1}$. Figure 28 compares these values to those measured in simple bubble columns and packed columns [108] (referred not to the total volume but to the liquid volume). This figure illustrates the advantages of downflow bubble columns, which have higher a_{L} values at low gas rates.

A *liquid-phase mass-transfer coefficient* $k_{\mathrm{L}} \approx 3.7 \times 10^{-4}$ m/s has been calculated by plotting the volumetric mass-transfer coefficient $k_{\mathrm{L}}\,a$ versus the volumetric gas holdup [110] and the bubble size stated above. Somewhat lower estimates, up to 3×10^{-4} m/s, have been reported in [109], [112]. However, the mass-transfer coefficient k_{L} cannot be measured directly, and large uncertainties are to be expected. The volumetric mass-transfer coefficients $k_{\mathrm{L}}\,a$ measured in bubble columns at equal gas holdups are roughly the same. Because of the very different volumetric gas flow rates in upflow and downflow bubble columns, different gas conversions are achieved; Figure 29 compares these figures for sulfite oxidation with air [110].

Data on the axial back-mixing of the gas phase have been reported [111]. At gas rates of $u_{\mathrm{G}} = 0.001 - 0.01$ m/s, the dispersion coefficient takes on constant high values: $D_{\mathrm{G}} \approx 0.2\,\mathrm{m}^2/\mathrm{s}$ ($d_{\mathrm{t}} = 0.025$ m, $u_{\mathrm{L}} = 0.334$ m/s, $\varepsilon_{\mathrm{G}} = 0.025 - 0.09$).

Back-mixing of the liquid phase under comparable conditions is also markedly less than in normal bubble columns [113].

Examples. STEINER and HERBRECHTSMEIER studied the *oxidation of sulfite solutions* with air in the downflow bubble column, finding a twelvefold higher depletion than with a simple bubble column (Fig. 29) [110].

A process for the *absorption of gases containing nitrogen oxides* has been reported [114]. Virtually complete conversion can be obtained through the use of a downflow bubble column 3 m high.

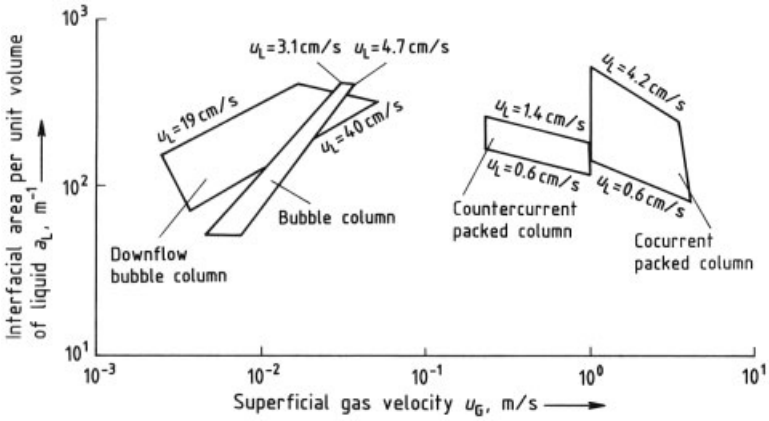

Figure 28. Comparison of mass-transfer area per unit liquid volume for various sparged devices as a function of gas velocity, with liquid velocity as parameter, according to [108]

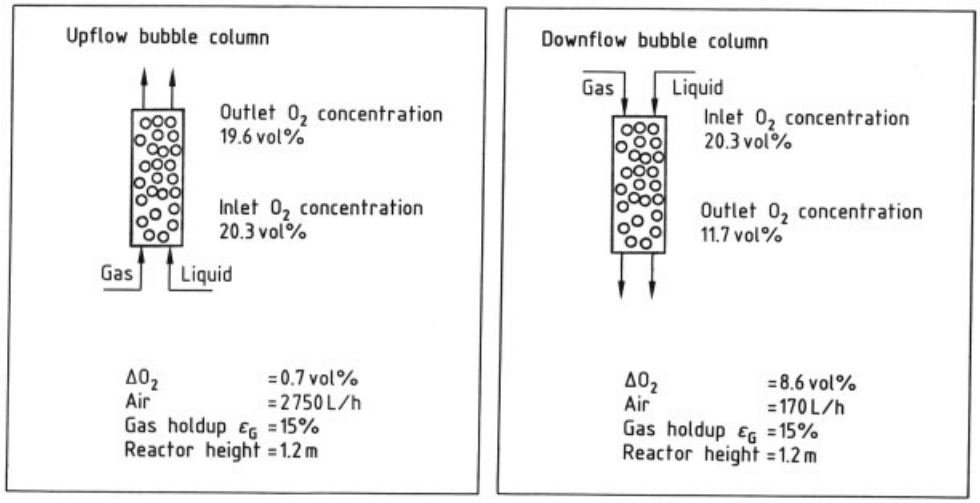

Figure 29. Comparison of oxygen depletion in upflow and downflow bubble columns for sulfite oxidation with air [110] $T = 22\,^{\circ}C$; $[SO_3^{2-}] = 0.4 - 0.8$ mol/L; $[Co^{3+}] = 7 \times 10^{-6}$ mol/L; pH = 8.0

The *degradation of organic contaminants by ozonolysis* is a well-known method of water treatment. For economic and safety reasons, virtually complete depletion of the ozone is desirable, which can be achieved in downflow bubble columns as reactors [115]. No danger of fouling exists in these devices, and high liquid throughputs can be handled. Figure 30 is a flow sheet of the entire process. Only a single theoretical mass-transfer unit can be realized, but this drawback can be overcome by the proposed use of a reactor cascade [115]. The phases are led through the cascade countercurrently.

4. Jet Loop Reactors

Jet loop reactors are among the most versatile gas – liquid contactors. The momentum of the liquid jet issuing from the nozzle enhances internal circulation and opposes demixing of the phases (distribution method C in Fig. 1). The liquid jet can be utilized to suck in, compress, and disperse fresh or recycle gas (Figs. 31, 32, 33, 34). The liquid-jet data are important process parameters. The liquid volumetric flow rate, velocity, and power can be varied over wide ranges. Finally, the size of the draft tube and the upper

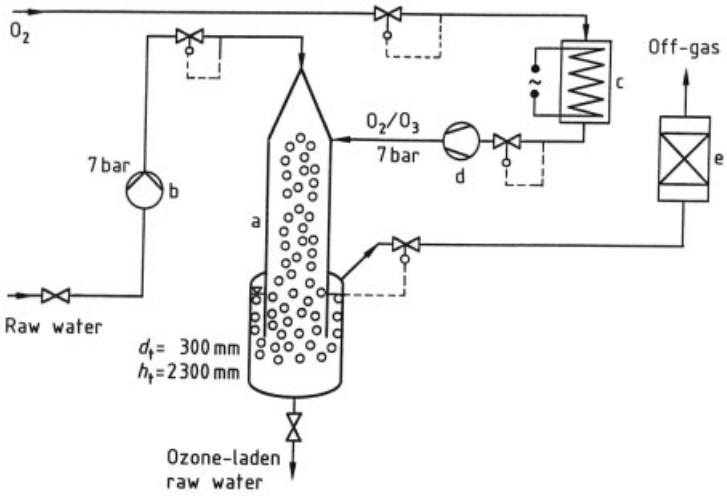

Figure 30. Plant with downflow bubble column for ozone treatment of water
a) Downflow reactor; b) Pressurizing pump; c) Ozone generator; d) Compressor; e) Deozonizer

flow-reversal zone strongly affect fluid dynamics and gas separation. Other possible variations are offered by the nozzle configuration (Figs. 32, 33, 34).

The four examples in Figure 31 illustrate options for the direction flow pattern phases. In all cases the gas is incorporated into the liquid via the nozzle located in the gas space. The liquid jet entrains gas bubbles until the nozzle orifice is closed by the rising liquid surface. The incorporation of more gas submerges the nozzle and blocks the gas inlet, the surface level then drops again; this self-regulating mechanism enables the gas holdup to be controlled.

A jet loop reactor (also called a gas-circulation reactor) [116] without net gas or liquid throughput is shown in Figure 31 A. Both phases are let in at the top and discharged at the top (the gas phase is consumed to a higher or lower degree). This corresponds to dispersion method C of Figure 1.

If the gas is under pressure, it can also be let in at the bottom to intensify circulation. The result is a net gas rate, as in the bubble column (Fig. 31 B); here, distribution methods A and C of Figure 1 are combined.

Figure 31 C shows a combination of sparging methods B and C in Figure 1. The liquid is fed at the top and discharged at the bottom. This jet loop reactor has an additional net flow of liquid, as in a downflow bubble column.

A combination of all three distribution methods (bubble column, downflow bubble column, and jet loop) is shown in Figure 31 D. The process characteristics of one sparging type will predominate, depending on the selected gas and liquid flow rates. At high gas flow rates, for example, the liquid surface level rises above the nozzle orifice. The liquid jet then no longer entrains gas bubbles, serving only to drive the circulation and disperse the bubbles. This versatile type of distribution can be further refined through variation of the nozzle position and the use of self-priming ejectors (Figs. 32, 33, 34). To evaluate a design, the essential process parameters must be estimated, which is not always feasible because of the many possible variations. For the basic forms shown in Figure 31, however, some information can be derived from a power balance (Section 4.2).

4.1. Design and Applications

Loop Reactors with Downflow Liquid Jets. Figure 32 illustrates several loop reactors with downward-pointing nozzles. These reactors are even suitable for suspension catalysis. If the pump or feedstream is cut off or fails, the nozzle drains clear, and the danger of the nozzle being plugged by the suspended catalyst is thus reduced. Another advantage is the long gas res-

idence time. From the inlet at the top, the gas circulates through the loop at least once. Moreover, the devices are designed so that the gas is internally recycled. This is important for the complete conversion of gases containing little or no inerts.

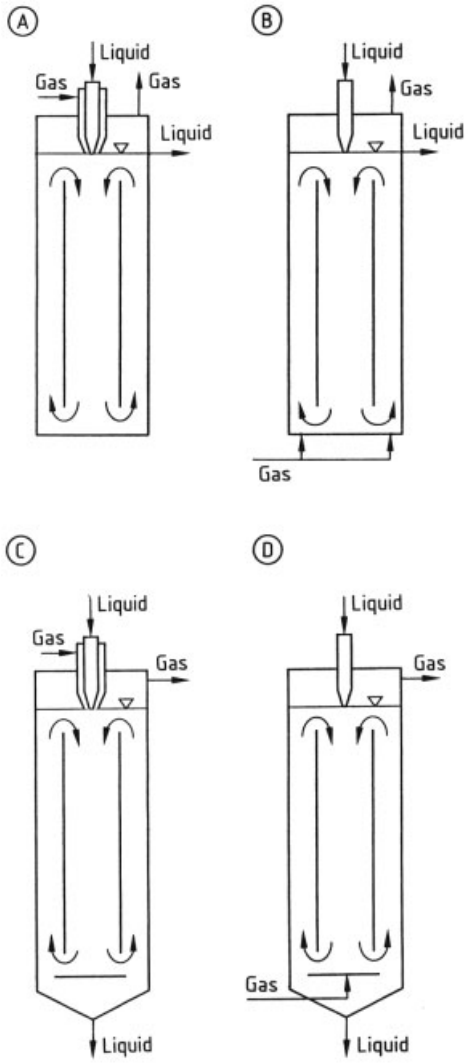

Figure 31. Options for phase routing in the "gas-circulation" type of jet loop reactor
A, C) With surface gas sparging; B, D) With pressure sparging (with gas throughput); C, D) With bottom outlet for liquid, inlet at top (with liquid throughput)

In the gas- circulation reactor of Figure 32 A (see also Fig. 31) [116], the gas can also be let in at the bottom of the reactor, independently of the nozzle, if the gas is available at reactor pressure. For a given jet power, this design offers much higher gas holdups and better mass-transfer performance (Sections 4.5 and 4.6). The jet only has to supply the recycle gas. Another marked increase (up to a factor of two) in the gas holdup is achieved by installing a *momentum-transfer tube* in the reactor. This can be submerged (Fig. 33 B) or can extend above the liquid surface (Fig. 33 C).

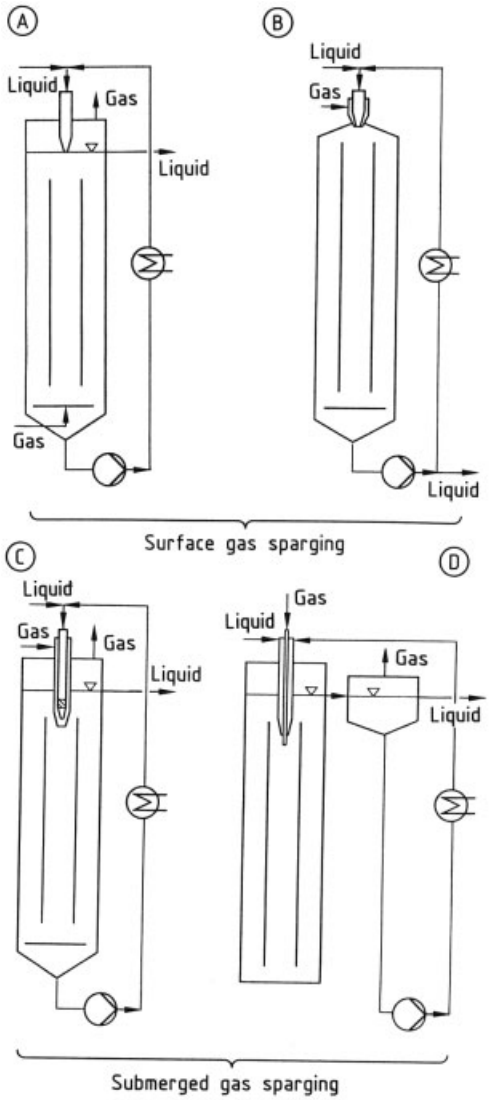

Figure 32. Types of jet loop reactors with downward liquid jet
A) Gas-circulation reactor with pressure sparging; B) Gas-circulation reactor without connected gas space; C) Gas-circulation reactor with submerged nozzle; D) "Compact" reactor with annular space for liquid injection

To prevent separation of the gas phase, the nozzle can be built directly into the reactor top (Fig. 32 B) [117]. Gas bubbles separating in this zone are immediately entrained by the liquid jet and redispersed into the circulating flow.

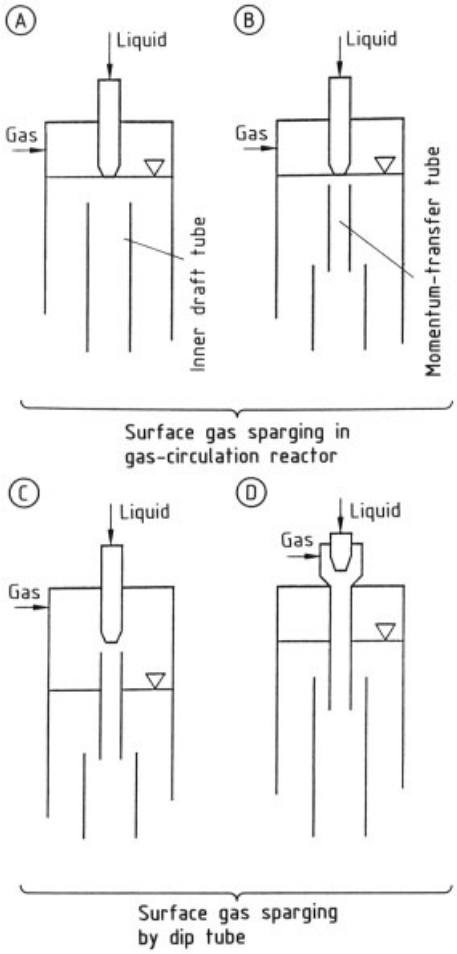

Figure 33. Options for spontaneous gas sparging from top Surface sparging in gas-circulation reactor without (A) and with (B) momentum-transfer tube; dip-tube sparging without (C) and with (D) self-priming ejector

The submerged nozzle in Figure 32 C can either accept pressurized gas from outside the system [118] or suck the gas in. Internal gas recycle is also possible. The suction of the nozzle can be enhanced by applying a swirl to break up the liquid jet, provided the liquid nozzle orifice is set back somewhat to the rim of the nozzle. The ejectors and ejector nozzles discussed in Chapter 2 are suitable for deeper submergence (see also Fig. 34 B and C).

In the jet loop reactor proposed by RÄBIGER and coworkers, the liquid is fed in via an annular nozzle (Fig. 32 D) [119], [120]. Gas can be drawn in via the center tube (ejector fashion) or supplied under pressure (injector fashion). For application of this reactor type in wastewater treatment see [121], [122].

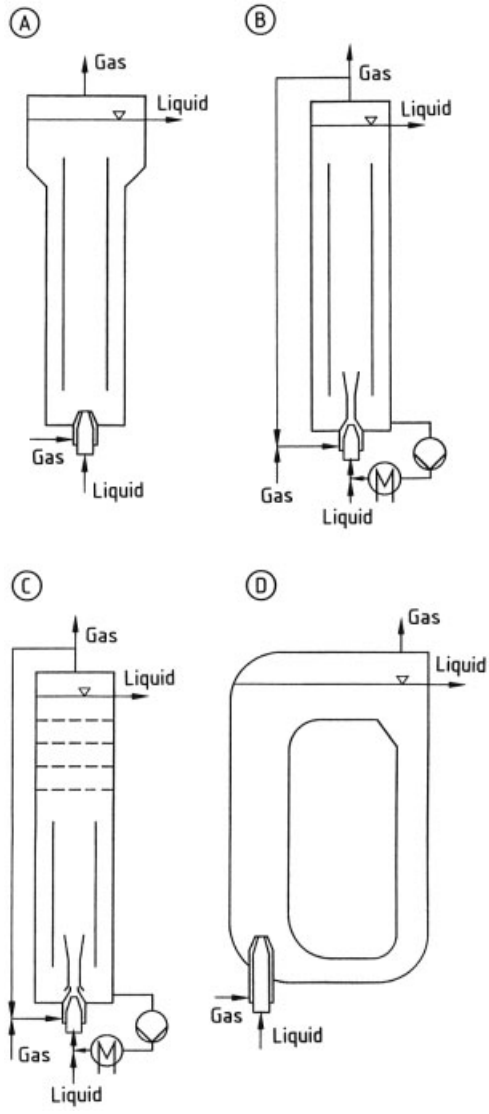

Figure 34. Design options for loop reactors with upward liquid jet
A) With expanded head for gas separation; B) With gas recycle via a self-priming ejector; C) With gas recycle via an ejector jet nozzle and perforated plates; D) With external recycle tube

Submerged nozzles supply the gas in the loop flow. The penetration depth of the jet differs. The reactor is thus easier to start up and the circulation flow can be build up in a simpler way. This is particularly important in batch processes. In principle, submerged nozzles represent an intermediate stage between surface sparging (Fig. 32 A and B) and pressurized gas sparging through nozzles at the bottom of the reactor (Fig. 34).

In the gas- circulation reactor of Figure 33, gas sparging takes place through the free surface. If a momentum-transfer tube is used (Fig. 33 B), gas enters the circulating flow at a greater depth. This arrangement functions even when the liquid level drops and the momentum-transfer tube extends into the gas space (Fig. 33 C). In Figure 33 D, the tube is led outside the reactor, so that gas can be delivered directly from outside without any mixing with recycle gas. The last two types of gas sparging (Fig. 33 C and D) are also referred to as dip-tube sparging designs.

Jet Loop Reactors with Upflow Liquid Jet (Fig. 34). In the second major variant of the jet loop reactor, the nozzle points upward. This design is closely related to the airlift loop reactor (Section 2.14). The liquid jet mainly produces smaller gas bubbles so that conversion of the gas phase can be improved. On the other hand, the circulation velocity is increased. At least a portion of the gas is thereby driven through the reactor faster than in airlift reactors, with the possible result of lower conversion; this danger exists particularly in the reactor of Figure 34 A, which uses a jet nozzle. The widened separation zone at the top can reduce gas recirculation or cut it off altogether; the result is improved mixing of the liquid phase because the circulation velocity increases with increasing gas holdup in the downcomer. Gas recycle is recommended whenever part of the gas leaves the column unconverted; it can be accomplished without a mechanical recycle-gas compressor if an ejector or an ejector jet nozzle is employed (Fig. 34 B and C). The ejector jet nozzle offers a higher compression efficiency than the ejector and produces larger interfacial areas [12]. From the chemical reaction engineering standpoint the combination of a loop reactor with a series of perforated plates is very interesting (Fig. 34 C). The lower part (loop reactor) exhibits the residence-time distribution of a stirred tank. Back-mixing is suppressed in the second section (perforated plates). For higher-order reactions, the conversion of both liquid and gaseous components can be increased in this way. With pure gases, recycle ensures adequate distribution because the gas flow rate is sufficient for an even gas load of the perforated plate.

Figure 34 D shows a reactor (analogous to the airlift loop of Fig. 22 D) with external recirculation. This device has an operational behavior comparable to that of reactors with internal circulation. Its advantages include better gas separation and simpler heating or cooling facilities. The accessible heat-transfer area is larger, and a conventional heat exchanger can be integrated directly into the loop.

The most important *characteristics* of jet loop reactors with upward-pointing nozzles can be summed up as follows:

1) They are particularly suitable for higher gas throughputs or when the gas has a high content of inerts
2) They have larger interfacial areas than bubble columns, especially with system with hindered coalescence
3) They offer more intensive back-mixing than bubble columns
4) They are less suitable for suspension catalysis, because the nozzle can become plugged

4.2. Typical Dimensions

In jet loop reactors, *height-to-diameter ratios* h_t/d_t of 5 to 20 are common. When several nozzles are used along with internal tubes, arbitrarily small height-to-diameter ratios can be achieved. Values larger than 20 are also seen in high-pressure operation and in pilot plant reactors.

The optimal *diameter* d_i *of the internal tube* is dictated by the direction of flow. If flow in the tube is *downward*, tubes with a diameter ratio d_i/d_t of 0.2 – 0.5 are suggested [116], [119]. The narrower internal tubes have the principal advantages of higher gas holdup and better mass-transfer at low energy dissipation rate (up to 1 kW/m^3). As jet power increases, the wider tubes become better in these respects [119], [123].

For *upward flow*, BLENKE and coworkers determined the optimal internal tube diameter as $d_i/d_t = 0.59$ [124]; this result applies to single- and two-phase reactors.

A crucial parameter of the jet loop reactor is the *nozzle diameter* d_n. Common values are in the range of $d_n/d_t = 0.02 - 0.1$. For a given jet power, large nozzles are more efficient than smaller ones for coalescing systems. In systems with hindered coalescence, in contrast, this relationship can be reversed.

4.3. Energy Balance

In the general case of Figure 31 D (combination of bubble column, downflow bubble column, and jet loop reactor), a total of five mechanical power terms can be identified [125]. These can be referred to the reaction volume

$$V_R = \frac{\pi}{4} d_t^2 h_R \tag{4.1}$$

Three types of power are *delivered to the reactor*:

1) Jet thrust power e_{thrust} per unit volume:

$$e_{thrust} = f_i \varrho_L \frac{v_n^2 v_{L,i}}{h_R} \left(\frac{d_n}{d_t}\right)^2 \tag{4.2}$$

where f_i is the fraction of cross-sectional area of the inner tube and v_n is the nozzle velocity

2) Power input per volume due to liquid flow e_L (as in a downflow bubble column) :

$$e_L = \Delta\varrho g \varepsilon_G u_L \tag{4.3}$$

3) Power input per unit volume due to gas flow e_G (as in a bubble column; holds approximately only for small pressure changes):

$$e_G \approx \Delta\varrho g \,(1-\varepsilon_G)\, u_G \tag{4.4}$$

This power is *transformed to heat* by two mechanisms:

1) Power dissipation per unit volume due to circulation flow:

$$e_{circ} = -\zeta f_i \bar{\varrho} \frac{v_{L,i}^3}{2h_R} \tag{4.5}$$

2) Power dissipation per unit volume due to friction between phases (slip power):

$$e_{slip} = -\Delta\varrho g \varepsilon_G \,(1-\varepsilon_G)\, v_{rG} \tag{4.6}$$

A combination of these terms gives the balance equation:

$$e_{thrust} + e_G + e_L + e_{slip} + e_{circ} = 0 \tag{4.7}$$

In general, the quantities $v_{L,i}$ (i.e., e_{circ}) and ε_G (i.e., e_{slip}) are unknown, so direct evaluation is impossible.

4.4. Mixing Behavior and Fluid Dynamics

The flow processes in jet loop reactors are particularly crucial for the mixing and residence-time distribution of both phases. The investigation of the relationship between mixing time and liquid circulation time showed that complete homogenization of the liquid phase requires ca. ten passes [126].

The *residence-time distribution of the liquid* in the jet loop reactor has been investigated both experimentally and theoretically [127], [128]. Values of dispersion coefficients in the liquid are presented in [118], [128]. The crucial parameter for mixing is the internal circulation flow generated by the liquid let in through the nozzle. In certain cases, this quantity can be estimated from the energy balance (Eq. 4.7).

The *residence-time distribution of the dispersed gas phase* can be found in [129]. The dispersion coefficients are not substantially different from those of the liquid phase.

Fluid Dynamics of Single-Phase Flow. The simplest formulation is that of single-phase flow. For $e_G = 0$, $e_{slip} = 0$, $e_L = 0$, the following holds for liquid circulation flow

$$v_{L,i} d_t = \sqrt{\frac{2}{\zeta f_i}}\, v_n d_n \tag{4.8}$$

The drag coefficient of circulation flow ζ can be found in [118], [130–132]. Typical values for bottom gas feed are $\zeta = 4$; for top gas feed, $\zeta \approx 0.25 - 2$.

Fluid Dynamics of Two-Phase Flow. In two-phase flow the momentum balance can be solved for the circulation flow $v_{\mathrm{L,\,i}}$ only if the gas holdup ε_{G} is known, which is not normally the case. Only in the gas-circulation reactor (Fig. 32 A, B) can the gas holdup be definitely specified within a certain range. Under the assumption of low gas holdup ε_{G}, for example, the following implicit relation is reported [123]:

$$(v_{\mathrm{n}} d_{\mathrm{n}})^2 = \left\{ \frac{\zeta f_{\mathrm{i}}}{2} v_{\mathrm{L,i}}^2 + \frac{\Delta\varrho}{\varrho_{\mathrm{L}}} g h_{\mathrm{R}} \frac{\varepsilon_{\mathrm{G}} (v_{\mathrm{rG}} - u_{\mathrm{L}}) - u_{\mathrm{G}}}{v_{\mathrm{L,i}}} \right\} d_{\mathrm{t}}^2 \quad (4.9)$$

The resistance coefficients ζ obtained for single-phase flow can be used to a good approximation. Figure 35 shows a logarithmic plot of Equation (4.9) for $u_{\mathrm{L}} = 0$ and $u_{\mathrm{G}} = 0$. The liquid velocities in the two-phase regime are always lower than in single-phase flow. If the velocity goes below a minimum value, the flow becomes unstable and stops, as shown by the nonlinear behavior of the curves at low velocities. Gas sparging then takes place only in the upper part of the internal tube. These features are illustrated in Figure 35. The minimum flow velocities $v_{\mathrm{L,\,i,\,min}}$ are a factor of $\sqrt{3}$ smaller than the single-phase velocities. This means that all possible velocities in two-phase flow are in the range

$$\frac{1}{\sqrt{3}} \leq \frac{v_{\mathrm{L,i}} d_{\mathrm{t}}}{\sqrt{\frac{2}{\zeta f_{\mathrm{i}}}} v_{\mathrm{n}} d_{\mathrm{n}}} \leq 1$$

The minimum flow velocity can also be obtained from Equation (4.9):

$$v_{\mathrm{L,i,min}} = \sqrt[3]{\frac{\Delta\varrho/\varrho_{\mathrm{L}}}{\zeta f_{\mathrm{i}}} g h_{\mathrm{R}} [\varepsilon_{\mathrm{G}} (v_{\mathrm{rG}} - u_{\mathrm{L}}) - u_{\mathrm{G}}]} \quad (4.10)$$

At high gas velocities u_{G} or when the nozzle is at the bottom of the reactor (Fig. 34 A), gas holdup cannot be freely selected. Instead, it adjusts itself as a function of fluid-dynamic conditions. At present, flow velocities cannot be calculated in advance.

BOHNER's measurements for the jet loop reactor are plotted in Figure 36 in the form

$$\bar{v}_{\mathrm{L,c}} d_{\mathrm{t}} = f(v_{\mathrm{n}} d_{\mathrm{n}}, u_{\mathrm{G}})$$

[133], [134]. Two regions can be identified. At low jet velocities v_{n}, the jet loop behaves like an airlift loop reactor (Section 2.14). The liquid circulation velocity is almost independent of jet velocity. Only at larger values does $v_{\mathrm{L,\,c}}$ increase linearly with v_{n} as in single-phase flow [133–135]. Investigations on radial velocity profiles in loop reactors are found in [135].

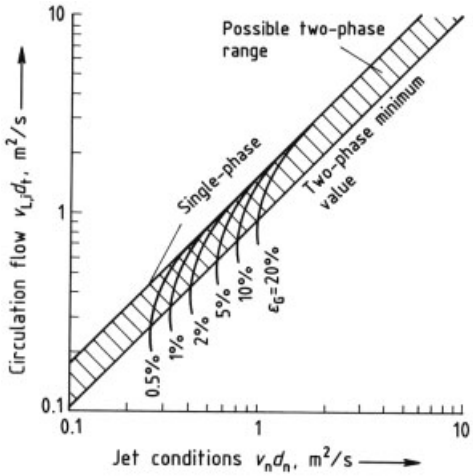

Figure 35. Circulation flow rate in gas-circulation reactor as a function of jet conditions and gas holdup, calculated with Equation (4.9)
Assumptions: $\zeta = 2.5$; $v_{\mathrm{rG}} = 0.23$ m/s; Geometric dimensions: $d_{\mathrm{t}} = 0.3$ m; $d_{\mathrm{h}} = 0.015$ m; $h_{\mathrm{t}} = 2.0$ m; $f_{\mathrm{i}} = 0.25$

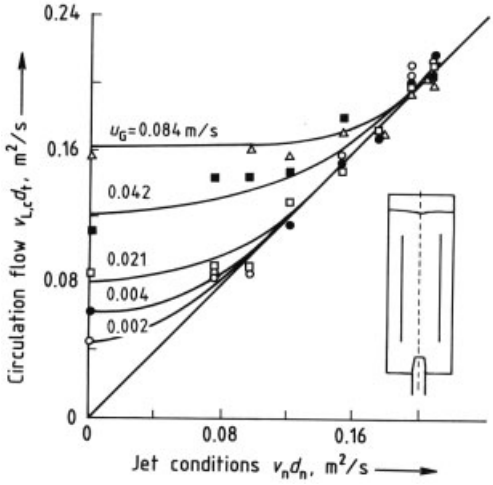

Figure 36. Measured circulation flow in pressure-sparged jet loop reactor as a function of jet conditions, with gas velocity as parameter [133]
$d_{\mathrm{t}} = 0.29$ m; $h_{\mathrm{t}} = 2.0$ m; $f_{\mathrm{i}} = 0.35$

4.5. Gas Holdup

In the *gas-circulation reactor* (Figs. 31 and 32 A and B), the gas holdup can be set arbitrarily

within certain limits. For a given jet velocity v_n, the maximum values $\varepsilon_{G,max}$ can be calculated from the power input by the liquid jet

$$P_n = \frac{\varrho_L}{2} v_n^3 F_n \text{ where } F_n = \frac{\pi}{4} d_n^2 \quad (4.11a)$$

or the jet power per unit volume

$$e_n = \frac{P_n}{V_R} = \frac{\varrho_L}{2} \cdot \frac{v_n^3}{h_R} \left(\frac{d_n}{d_t}\right)^2 \quad (4.11b)$$

The equations reported by TEBEL and ZEHNER are presented here in simplified form [123]. The maximum specific energy dissipation rate caused by the slip between the two phases (Eq. 4.6) is given by

$$e_{slip,max} = \frac{4}{3^{1.5}} \sqrt{\frac{2}{\zeta f_i}} e_n \frac{d_n}{d_t} \quad (4.12)$$

which can be solved as follows for the maximum gas holdup:

$$\varepsilon_{G,max} = \frac{2}{3^{1.5}} \sqrt{\frac{2}{\zeta f_i}} \cdot \frac{2e_n \frac{d_n}{d_t}}{\Delta \varrho g v_{rG}}$$

$$= \frac{2}{3^{1.5}} \sqrt{\frac{2}{\zeta f_i}} \cdot \frac{2P_n \frac{d_n}{d_t}}{\Delta \varrho g v_{rG} V_R} \quad (4.13)$$

Equation (4.13) is compared with measured values in Figure 37. The lowest gas holdups are obtained in the coalescing system water – air. Even tiny amounts of methanol reduce the tendency to coalesce. The primary gas bubbles generated by the jet retain approximately the same size over the whole apparatus because they do not coalesce. This reduces their slip velocity v_{rG} so that much higher gas holdups and interfacial areas can be obtained.

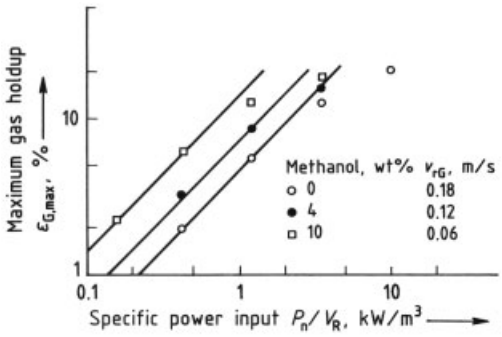

Figure 37. Comparison of measured and calculated maximum gas holdup as a function of specific jet power in gas-circulation reactor
System: water – air with added methanol; measured values after [123]; calculations with Equation (4.13)
$d_t = 0.14$ m; $h_t = 1.32$ m; $d_i = 0.055$ m; $d_n = 4.9$ mm

More complex relationships apply if pressurized gas is let in at the bottom of the gas-circulation reactor. The gas holdup then sets itself, analogously to behavior in a bubble column, an airlift loop reactor (Sections 2.9 and 2.14),

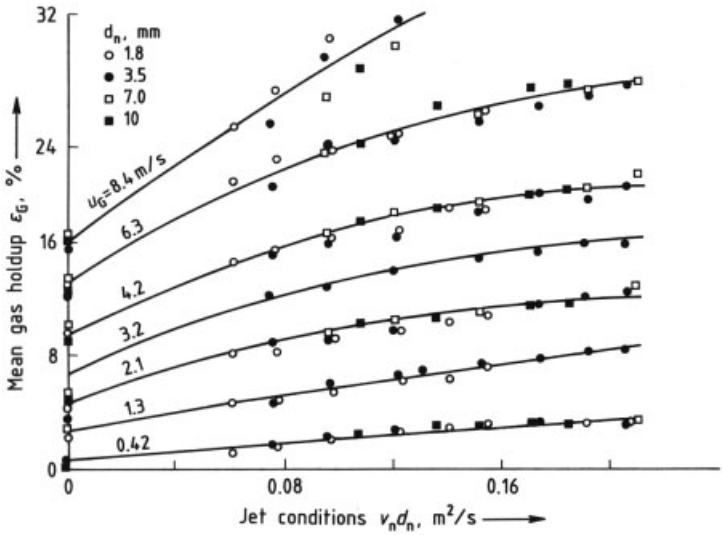

Figure 38. Gas holdup measured in the pressure-sparged jet loop reactor [133] versus jet conditions at various gas velocities
$h_t = 2$ m; $d_t = 0.29$ m; $f_i = 0.33$

or the ordinary loop reactor (Fig. 34 A). Typical measured values for this type of gas sparging are presented in Figure 38. As the gas rate increases, gas holdup increases rapidly. The jet velocity, by contrast, has relatively little effect.

ZEHNER and THELEN obtained the expression

$$\frac{e_{\mathrm{slip}}}{2e_{\mathrm{n}}\frac{d_{\mathrm{n}}}{d_{\mathrm{t}}}} = f\left(\frac{e_{\mathrm{G}}}{2e_{\mathrm{n}}\frac{d_{\mathrm{n}}}{d_{\mathrm{t}}}}\right) \tag{4.14}$$

for jet loop reactors with pressurized gas sparging [125]. Figure 39 shows the gas holdup for different reactor types and sparging types, based on this relation. To within measurement error, the same values are obtained for the gas-circulation reactor with pressurized gas sparging (Fig. 31 B) and for the jet loop reactor (Fig. 34). These values are fitted well by the correlation

$$\frac{e_{\mathrm{slip}}}{2e_{\mathrm{n}}\frac{d_{\mathrm{n}}}{d_{\mathrm{t}}}} = 1.5\left(\frac{e_{\mathrm{G}}}{2e_{\mathrm{n}}\frac{d_{\mathrm{n}}}{d_{\mathrm{t}}}}\right)^{0.8} \tag{4.13a}$$

which can be solved directly for the gas holdup:

$$\varepsilon_{\mathrm{G}} = 1.5\left(\frac{2P_{\mathrm{n}}\frac{d_{\mathrm{n}}}{d_{\mathrm{t}}}}{\Delta\varrho g v_{\mathrm{rG}} V_{\mathrm{R}}}\right)^{0.2}\left(\frac{u_{\mathrm{G}}}{v_{\mathrm{rG}}}\right)^{0.8} \tag{4.13b}$$

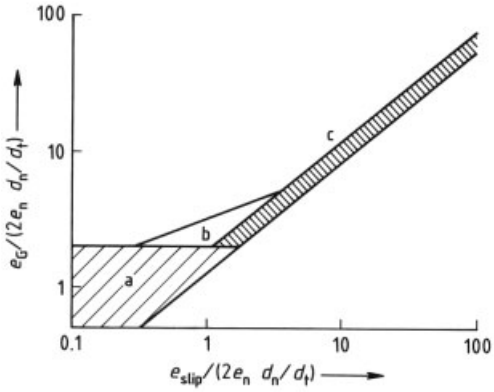

Figure 39. Relationship between slip power ϱ_{slip}, jet power ϱ_{n}, and gas compression power ϱ_{G} for determination of gas holdup
a) Surface sparging in gas-circulation reactor; b) Transition between surface and pressure sparging; c) Pressure sparging in gas-circulation reactor and normal jet loop reactor

4.6. Mass Transfer

The mean bubble diameter in a sparged reactor is always the result of distribution and coalescence processes. In the *easily coalescing water – air system*, the bubble diameter corresponds essentially to the local energy dissipation rate, a quantity that is distributed very unevenly over the volume in jet loop reactors. Zones of particularly high energy-dissipation rate include the immediate action region of the liquid jet and, to a lesser degree, the regions of loop flow reversal. This is the reason why the smallest bubbles are observed near the jet in the compact reactor (see Fig. 32 D) [120]. As Figure 40 shows, bubble size decreases from ca. 3 mm to almost 2 mm with increasing energy dissipation rate $P_{\mathrm{n}}/V_{\mathrm{R}}$. In the other much larger regions, the bubbles quickly coalesce to bigger (3 – 4 mm) units. Jet loop reactors accordingly do not feature smaller air-in-water bubbles, on average, than bubble columns or downflow bubble columns operated in the homogeneous flow regime. For a given gas holdup, comparable mass-transfer should therefore be expected. The relationships among the mean bubble diameter (Sauter diameter) d_{bS}, the gas holdup ε_{G}, the specific interfacial area a, and the volumetric mass-transfer coefficient $k_{\mathrm{L}}\,a$ have been pointed out in Section 3.3. These considerations lead to the following guideline values for the water – air system:

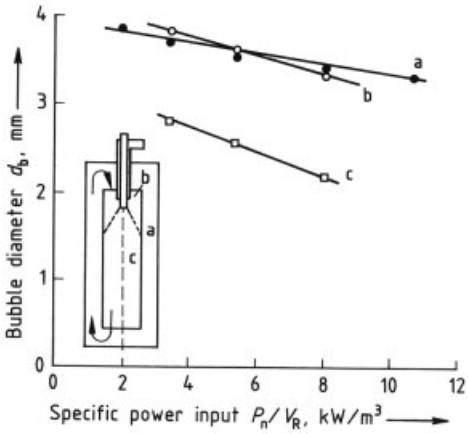

Figure 40. Bubble sizes in the compact reactor (system: water – air)
$d_{\mathrm{t}} = 0.1$ m; $h_{\mathrm{t}}/d_{\mathrm{t}} = 5.9$; $d_{\mathrm{n}} = 5$ mm; $d_{\mathrm{i}}/d_{\mathrm{t}} = 0.6$

Usual specific energy dissipation rates:
$P_{\mathrm{n}}/V_{\mathrm{R}} \approx 1 - 10\,\mathrm{kW/m^3}$
Mean bubble diameter (Sauter diameter):
$d_{\mathrm{bS}} \approx 3.5$ mm
Maximum gas holdup: $\varepsilon_{\mathrm{G}} \approx 6 - 30$ %

Special interfacial area: $a \approx 100 - 600\,\mathrm{m}^{-1}$
Volumetric mass-transfer coefficient: $k_\mathrm{L}\,a \approx 0.04 - 0.2\,\mathrm{s}^{-1}$

If liquid mixtures and ionic or detergent solutions exhibit a *noncoalescing behavior*, much higher gas holdups and smaller bubble diameters (significantly less than 1 mm) can be achieved. The volumetric mass-transfer coefficients and specific interfacial areas behave in a similar way; in systems with hindered coalescence they may be a factor of 5 to 10 higher than the water – air values. A compilation of volumetric mass-transfer coefficients in various types of sparged apparatus can be found in [136].

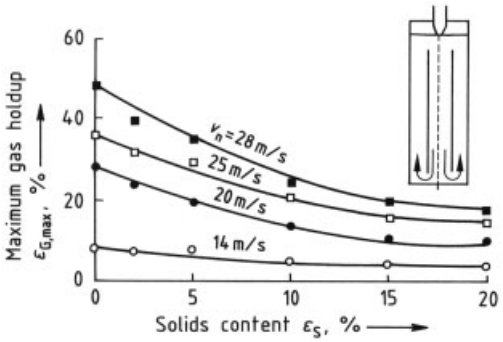

Figure 41. Effect of solids on gas holdup in the gas-circulation reactor
System: 1 wt % NaCl – air – glass spheres; $d_\mathrm{P} = 0.075 - 0.15$ mm

4.7. Three-Phase Loop Reactor

When solids are suspended in sparged loop reactors the same engineering considerations are necessary as in slurry bubble columns (Section 2.13). Many workers have studied the effect of solid particles on fluid dynamics and mass-transfer performance [76], [137–139].

The fluid-dynamic principles of solid – liquid systems are comparable to those of gas – liquid systems (Sections 4.3 and 4.4) [132], [140]. These considerations have been extended to threephase systems so that theoretical models are available for complex multiphase flow [120], [123], [141]. In principle, the solid phase is accounted for by a supplemental energy term for the slip power dissipation of the particle swarm (Section 4.3). How interactions between phases influence individual slip velocities is not clear. For example, KÜRTEN and coworkers examined the maximum possible gas holdup in a gas-circulation reactor with gas sparging at the surface [76]. As Figure 41 shows, the solids content ε_S has a strong effect that cannot be accounted for merely by the additional slip power dissipation of fine particles. Instead, the slurry must be assumed to yield larger gas bubbles because of its higher apparent viscosity. The higher slip velocity of these larger bubbles might then explain the marked dependence on solids concentration.

RÄBIGER [138] and WACHSMANN [139] also studied the effect of solids. At constant energy dissipation rate and constant volumetric gas flow rate, the dependences are roughly similar to those found in [76]. Only for low solids and gas holdups does a slight increase in gas holdup occur relative to two-phase systems.

This has been explained by bubble breakup by large solid particles [142]. The effect should not occur below the critical Weber number

$$We = \frac{\varrho_\mathrm{S} d_\mathrm{S} v_\mathrm{b}^2}{\sigma} = 3$$

However, this statement partially contradicts RÄBIGER's results [138]. Technically, these discrepancies are insignificant. Up to a solids concentration of 10 vol %, no major differences exist in gas holdup and mass-transfer between normal and three-phase jet loop reactors. Higher volumetric particle concentrations do not, however, normally occur in jet loop reactors.

5. References

1. H. Gerstenberg, *Chem.-Ing.-Tech.* **47** (1975) no. 5, 209.
2. M. Bobik, *Chem.-Ing.-Tech.* **53** (1981) MS 922.
3. BASF, EP 254 180, 1991 (P. Zehner et al.).
4. Hoechst, DE-OS 2 855 263, 1978 (A. Riedel et al.).
5. R. Steiner, *Chem. Eng. Process.* **21** (1987) 1 – 8.
6. W.-D. Deckwer, J. Hallensleben, M. Popovic, *Can. J. Chem. Eng.* **58** (1980) 190.
7. H. Buchholz, Dissertation, Universität Hannover 1979.
8. K. Ruff, T. Pilhofer, A. Mersmann, *Chem.-Ing.-Tech.* **48** (1976) no. 9, 759 – 764.
9. G. Neubauer, T. Pilhofer, *Chem.-Ing.-Tech.* **50** (1978) no. 2, 115 – 116.

10. Mersmann, A., *Ger. Chem. Eng. (Engl. Transl.)* **1** (1978) 1.
11. P. Krötsch, *Fortschr. Verfahrenstech. Abt. D* **16** (1978) 389.
12. P. Zehner, *Chem.-Ing.-Tech.* **47** (1975) no. 5, 209.
13. H. Gerstenberg, *Chem.-Ing.-Tech.* **51** (1979) no. 3, 208 – 216.
14. Y. T. Shah, B. G. Kelkar, S. P. Godbole, W. D. Deckwer, *AIChE J.* **28** (1982) 353 – 379.
15. J. B. Joshi, Y. T. Shah, *Chem. Eng. Commun.* **11** (1981) 165 – 199.
16. K. Rietema, S. P. P. Ottengraph, *Trans. Inst. Chem. Eng.* **48** (1970) T 54.
17. J. R. Crabtree, J. Bridgwater, *Chem. Eng. Sci.* **24** (1969) 1755.
18. S. M. Bhavraju, T. W. F. Russel, H. W. Blanch, *AIChE J.* **24** (1978) 454.
19. K. Ueyama, T. Miyauchi, *AIChE J.* **25** (1979) 258 – 266.
20. J. B. Joshi, M. M. Sharma, *Trans. Inst. Chem. Eng.* **57** (1979) 244.
21. P. Zehner, *Ist. Chem. Eng.* **26** (1986) no. 1, 22 – 35.
22. A. Lübbert: "Mass Transfer with Chemical Reactions in Multiphase Systems," NATO Advanced Study Institute, Cesme/Izmir, Aug. 10 – 11, 1981.
23. J. H. Hills, *Trans. Inst. Chem. Eng.* **52** (1974) 1 – 9.
24. E. Kojima et al., *J. Chem. Eng. Jpn.* **13** (1980) 16.
25. M. Kraume, P. Zehner, *German/Japanese Symposium Bubble Columns,* Schwerte 1988, preprints.
26. R. Buchholz, K. Schügerl, *Eur. J. Appl. Microbiol. Biotech.* **6** (1979) 301 – 315.
27. E. Blaß, *Chem.-Ing.-Tech.* **60** (1988) no. 12, 935 – 947.
28. P. H. Calderbank, *Chem. Eng.* **45** (1976) CE 209.
29. O. Nagel, B. Hegner, H. Kürten, *Chem.-Ing.-Tech.* **50** (1978) no. 12, 934 – 944.
30. H. Unno, I. Inoue, *Chem. Eng. Sci.* **35** (1980) 1571.
31. K. Akita, F. Yoshida, *Ind. Eng. Chem. Proc. Des. Dev.* **13** (1974) 84 – 91.
32. T. Miyahara, Y. Matsuba, T. Takahashi, *Int. Chem. Eng.* **23** (1983) 517 – 523.
33. T. Miyahara, N. Naga, T. Takahashi, *Int. Chem. Eng.* **23** (1983) 524 – 531.
34. K. Koide et al., *Chem. Eng. Jpn.* **12** (1979) 98 – 104.
35. A. Mersmann, *Chem.-Ing.-Tech.* **61** (1989), no. 2, 97 – 104.
36. H. Wezorke, Dissertation, Universität Dortmund 1986.
37. R. Beinhauer, Dissertation, TU Berlin 1971.
38. Y. T. Shah, G. J. Stiegel, M. M. Sharma, *AIChE J.* **24** (1978) 369 – 400.
39. M. Kraume, P. Zehner, *Chem.-Ing.-Tech.* **61** (1989) no. 4, 332 – 333.
40. K.-H. Mangartz, T. Pilhofer, *VT, Verfahrenstech.* **14** (1980) no. 1, 40 – 44.
41. P. Zehner, G. Schuch, *Ger. Chem. Eng. (Engl. Transl.)* **8** (1985) 282 – 289.
42. G. Blasey, Dissertation, Universität Dortmund 1987.
43. P. Herbrechtsmeier, R. Steiner, *Chem.-Ing.-Tech.* **52** (1980) 468.
44. W. Hikita et al., *Chem. Eng. J.* **20** (1980) 59 – 67.
45. R. Nottenkämper, A. Steiff, P. M. Weinspach, *Ger. Chem. Eng.* **6** (1983) 147 – 155.
46. H. F. Bach, T. Pilhofer, *Ger. Chem. Eng. (Engl. Transl.)* **1** (1978) 270. H. Buchholz, R. Buchholz, H. Niebeschütz, K. Schügert, *Eur. J. App. Microbiol. Biotechnol.* **6** (1978) 115.
47. K. Schügerl, J. Lücke, U. Oels, *Adv. Biochem. Eng.* **7** (1977) 1. G. Keitel, U. Onken, *Chem.-Ing.-Tech.* **54** (1982) no. 3, 262 – 263.
48. K. Akida, F. Yoshida, *Ind. Eng. Chem. Proc. Des. Dev.* **13** (1974) 84 – 91.
49. H. Kölbel, E. Borchers, H. Langemann, *Chem.-Ing.-Tech.* **33** (1961) no. 10, 668 – 675. W.-D. Deckwer, Y. Luisi, A. Zaidi, M. Ralek, *Ind. Eng. Chem. Proc. Des. Dev.* **10** (1980) 699.
50. M. H. Oyevaar, K. R. Westerterp, *Chem. Eng. Process.* **25** (1989) 85 – 98.
51. M. H. Oyevaar, R. Bos, K. R. Westerterp, *Chem. Eng. Sci.* **46** (1991) 1217 – 1231.
52. P. M. Wilkinson, L. v. Dierendonck, *Chem. Eng. Sci.* **45** (1990) 2309 – 2315.
53. A. Serizawa, I. Kataoka, I. Michiyoshi, *Int. J. Multiphase Flow* **2** (1975) 235 – 246.
54. W.-D. Deckwer, *Reaktionstechnik in Blasensäulen,* Salle und Sauerländer, Aarau 1985.
55. U. Oels, J. Lücke, R. Buchholz, K. Schügerl, *Ger. Chem. Eng. (Engl. Transl.)* **1** (1978) 115.
56. W.-D. Deckwer, R. Burchhart, G. Zoll, *Chem. Eng. Sci.* **29** (1974) 2177.
57. Y. Kawase, B. Halard, M. Moo-Young, *Chem. Eng. Sci.* **42** (1987) 1609 – 1617.
58. H. Hikita et al., *Chem. Eng. J.* **22** (1981) 61 – 69.
59. J. S. Cho, N. Wakao, *J. Chem. Eng. Jpn.* **21** (1980) 576 – 581.

60. S. P. Godbole, A. Schumpe, Y. T. Shah, N. L. Carr, *AIChE J.* **30** (1984) 213 – 220.
61. K. Akita, *Int. Chem. Eng.* **29** (1989) 127 – 135.
62. W. Kast, *Int. J. Heat Mass Transfer* **5** (1962) 329 –336.
63. W.-D. Deckwer, *Chem. Eng. Sci.* **35** (1980) 1341 –1346.
64. J. B. Joshi et al., *Chem. Eng. Commun.* **6** (1980) 257 –271.
65. A. N. Khoze et al., *J. Eng. Phys.* **20** (1971) 759 –763.
66. L. S. Aksel'rod, N. I. Vorotnikova, A. A. Kozlov, *Heat Transfer-Sov. Res.* **8** (1976) 25 – 33.
67. R. Wendt, Dissertation, Universität Dortmund 1983.
68. H.-J. Korte, Dissertation, Universität Dortmund 1987.
69. H.-J. Korte, A. Steiff, P.-M. Weinspach, *German/Japanese Symposium Bubble Columns,* Schwerte 1988, preprints.
70. R. Wendt, A. Steiff, P.-M. Weinspach, *Chem.-Ing.-Tech.* **55** (1983) no. 10, 796 – 797.
71. Y. T. Shah, C. A. Ratway, H. G. McIlvried, *Trans. Inst. Chem. Eng.* **56** (1978) 107 – 112.
72. K. Bernemann, Dissertation, Universität Dortmund 1989.
73. K. Koide, T. Yasuda, S. Iwamoto, E. Fukuda, *J. Chem. Eng. Jpn.* **16** (1983) 7 – 12.
74. S. Kara et al., *Ind. Eng. Chem. Proc. Des. Dev.* **21** (1982) 584 – 594.
75. Y. Kato et al., *Ist. Chem. Eng.* **13** (1979) 562 – 567.
76. H. Kürten, P. Zehner, *Ger. Chem. Eng. (Engl. Transl.)* **2** (1979) 220 – 227.
77. T. Sauer, Dissertation, Universität Paderborn 1986.
78. A. Yasunishi, M. Fukuma, K. Muroyama, *J. Chem. Eng. Jpn.* **19** (1986) 444 – 449.
79. K. Koide, A. Takazawa, M. Komura, H. Matsunaga, *J. Chem. Eng. Jpn.* **17** (1984) 459 – 466.
80. T. Matsumoto, N. Hidaka, S. Morooka, *AIChE J.* **35** (1989) 1701 – 1709.
81. H. Mürtz, Dissertation, Universität Dortmund 1990.
82. M. Fukuma, K. Muroyama, A. Yasunishi, *J. Chem. Eng. Jpn.* **20** (1987) 28.
83. E. Sada, H. Kumazawa, C.-H. Lee, H. Nakamura, *Ind. Eng. Chem. Proc. Des. Dev.* **26** (1987) 112.
84. K. Nguen-Tien, H. Patwari, A. Schumpe, W.-D. Deckwer, *AIChE J.* **31** (1985) 194.
85. H.-G. Springmann, A. Steiff, P.-M. Weinspach, *Chem.-Ing.-Tech.* **63** (1991) 162 – 163.
86. J. Kratochvil, K. Winkler, J. Zahradnik: *Coll. Czech. Chem. Commun.* **50** (1985) 48 – 60.
87. K. Muroyama, *German/Japanese Symposium Bubble Columns,* Schwerte 1988, preprints.
88. "Cyclohexane," *Hydrocarbon Processing* 1977, no. 11, 144.
89. U. Onken, P. Weiland, *Adv. Biotechnol. Processes* **1** (1983) 67 – 95.
90. M. Y. Chisti, *Airlift Bioreactors,* Elsevier Applied Science, London 1989.
91. P. Verlaan, J. C. Vos, K. van't Riet: *J. Chem. Technl. Biotechnol.* **45** (1989) 109 – 121.
92. R. A. Bello, C. W. Robinson, M. Moo-Young, *Can. J. Chem. Eng.* **40** (1984) 573 – 577.
93. P. Weiland, U. Onken, *Chem.-Ing.-Tech.* **52** (1980) 986 – 987.
94. P. Weiland, *Ger. Chem. Eng. (Engl. Transl.)* **7** (1984) 374 – 385.
95. Y. Kawase, M. Moo-Young, *Chem. Eng. Commun.* **40** (1986) 67 – 83.
96. T. Reith, Ph. D. Thesis, Universität Delft 1968.
97. W. Hirner, H. Blenke, *VT, Verfahrenstech.* **11** (1977) no. 5, 297 – 303.
98. K. Koide, H. Sato, S. Iwamoto, *J. Chem. Eng. Jpn.* **16** (1983) 407 – 413.
99. K. Koide et al., *J. Chem. Eng. Jpn.* **16** (1983) 413 – 419.
100. K. Nakao et al., *German/Japanese Symposium Bubble Columns,* Schwerte 1988, preprints.
101. K. Schügerl, *Bioreaktionstechnik,* vol. 2, Salle und Sauerländer, Aarau 1991.
102. P. K. Ouyoung, M. Y. Chisti, M. Moo-Young, *Chem. Eng. Res. Des.* **67** (1989) 451 – 456.
103. G. Müller, G. Sell, *DECHEMA-Monogr.* **86** (1980) 589.
104. S. J. Heijnen et al., *Chem. Eng. Technol.* **13** (1990) 202 – 208.
105. Y. Bando et al., *J. Chem. Eng. Jpn.* **21** (1988) no. 6, 607 – 612.
106. A. Ohkawa, Y. Shiokawa, N. Sakai, *J. Chem. Eng. Jpn.* **18** (1985) no. 6, 172 – 174.
107. A. Ohkawa, Y. Shiokawa, N. Sakai, N. Imai, *J. Chem. Eng. Jpn.* **18** (1985) no. 6, 466 – 469.
108. P. Herbrechtsmeier, H. Schäfer, R. Steiner, *Chem.-Ing.-Tech.* **56** (1984) MS 1221.
109. P. Herbrechtsmeier, H. Schäfer, R. Steiner, *Chem.-Ing.-Tech.* **53** (1981) MS 884.
110. P. Herbrechtsmeier, R. Steiner, *Chem.-Ing.-Tech.* **50** (1978) no. 12, 944 – 947.
111. A. Kulkarni, Y. T. Shah, *Chem. Eng. Commun.* **28** (1984) 311 – 326.
112. A. Ohkawa et al., *J. Chem. Eng. Jpn.* **20** (1987) no. 1, 99 – 101.

113. W. J. Albrecht, G. Schulze-Pillot, *Chem.-Ing.-Tech.* **50** (1987) no. 22.
114. R. Steiner, *Chem. Eng. Process.* **21** (1987) 1 – 8.
115. R. Steiner, *DECHEMA-Monogr.* **94** (1983) 164 – 197.
116. H. Kürten, P. Zehner, *Annual Conference of Chemical Engineering,* Straßburg, Oct. 1980.
117. BASF, EP 0 087 670, 1983 (H. H. Schuster, H. Dreher, J. Hambrecht).
118. H. Blenke in: Loop Reactors, Advances in Biochemical Engineering 13, Springer-Verlag, Berlin 1979.
119. N. Räbiger, A. Vogelpohl, *Chem.-Ing.-Tech.* **53** (1983) MS 1111.
120. N. Räbiger, Habilitationsschrift, Technische Universität, Clausthal 1988; *Praxiswissen thermische Verfahrenstechnik,* Verlag TÜV Rheinland, Köln 1988.
121. H. Loosen, *ZFL* **40** (1989) no. 9, 494 – 496.
122. B. Lohrengel, A. Vogelpohl, *Chem.-Ing.-Tech.* **62** (1990) MS 1856.
123. K. H. Tebel, P. Zehner, *Chem. Eng. Technol.* **12** (1989) 274 – 280.
124. H. Blenke, K. Bohner, W. Hirner, *Verfahrenstechnik (Mainz)* **3** (1969) no. 10, 444 – 452.
125. P. Zehner, H.-G. Thelen: "Mehrphasenströmung," Vortrag auf dem GVC-Fachausschuß, Bremen 1991.
126. A. Jaramillo, I. Adler, A. Fiechter, *Third European Congress on Biotechnology,* Munich, Sept. 10 – 14, 1984.
127. J. Lehnert, *Verfahrenstechnik (Mainz)* **6** (1972) 58.
128. H.-J. Warnecke, M. Weidenbach, J. Prüss, H. Langemann, *Chem.-Ing.-Tech.* **59** (1987) no. 6, 496 –499.
129. H.-J. Warnecke, D. Vaupel, I. Prüss, H. Langemann, *Chem.-Ing.-Tech.* **61** (1989 no. 10, 815 – 817.
130. H. Blenke, K. Bohner, S. Schuster, *Chem.-Ing.-Tech.* **37** (1965) no. 3, 289 – 294.
131. H. Blenke, K. Bohner, W. Pfeifer, *Chem.-Ing.-Tech.* **43** (1971) no. 1 – 2, 10 – 17.
132. P. Zehner, Habilitationsschrift, Universität Kaiserslautern 1988; *Fortschr.-Ber. VDI Z. Reihe 3,* 1988, no. 160.
133. K. Bohner, Dissertation, Universität Stuttgart 1971.
134. K. Bohner, H. Blenke, *Verfahrenstechnik (Mainz)* **6** (1972) no. 2, 50 – 57.
135. D. K. Jain et al., *Can. J. Chem. Eng.* **68** (1990) 1047 –1051.
136. H.-J. Warnecke, M. Geisendörfer, D. Ch. Hempel, *Chem. Eng. Technol.* **11** (1988) 306 – 311.
137. L.-S. Fan, S.-J. Hwang, A. Masuura, *Chem. Eng. Sci.* **39** (1984) no. 12, 1677 – 1688.
138. N. Räbiger, *Chem.-Ing.-Tech.* **57** (1985) no. 3, 248 –249.
139. U. Wachsmann, N. Räbiger, A. Vogelpohl, *VDI-Ber.* **607** (1986) 1537 – 1566. U. Wachsmann, N. Räbiger, A. Vogelpohl, *Ger. Chem. Eng. (Engl. Transl.)* **8** (1985) 411 – 418.
140. P. Zehner, *Chem.-Ing.-Tech.* **62** (1980) MS 850.
141. K. H. Tebel, P. Zehner, *Annual Meeting of the Process Engineers,* Straßburg, Sept 17 – 19, 1986.
142. J. C. Lee, *4th Proc. European Symp., Chem. React. Eng.,* 1971, p. 27.

Bubble Memories → Information Storage Materials
Buffing → Abrasives
Building Bricks → Construction Ceramics